Hybrid Access MAC Protocol in Wi-Fi: Analysis and Optimal Resource Allocation Policy Design

S. Arthi, *Student Member, IEEE,* Neelesh B. Mehta, *Fellow, IEEE,* and Chandramani Singh, *Member, IEEE*

***Abstract*—The hybrid medium access control (MAC) protocol, which was first adopted in the IEEE 802.11ax standard, combines contention-based random access (UORA) and contention-free scheduled access (SA) transmissions over orthogonal resource units (RUs). We present a novel fixed-point analysis of saturation throughput and average access delay of hybrid access that accounts for discrete rate adaptation, packet decoding errors, and scheduling. Using this analysis and Markov decision process (MDP) theory, we design a novel dynamic RU allocation policy (ODRAP) for hybrid access. Our analysis and policy design are the first to capture the dynamic flow of users between UORA and SA, and its dependence on the RU allocation. The existing literature has modeled UORA or SA, but not both, or has assumed a fixed number of SA users. We first develop the analysis when the number of packets reported in the buffer status report (BSR) of a user is a geometric random variable. We then present an iterative approach to handle application-specific general distributions. Our numerical results verify the accuracy of the analysis despite its simplicity. Furthermore, they highlight the impact of the number of allocated RUs on the scheduler. ODRAP optimally trades off the throughput with the access delay compared to several benchmark policies.**

***Index Terms*—IEEE 802.11ax, UORA, Hybrid access, Resource allocation, Saturation throughput, Access delay**

I. Introduction

Wireless fidelity (Wi-Fi) has evolved to facilitate connectivity for billions of devices and is the preferred choice for internet access among users. Wi-Fi is based on the IEEE 802.11 family of standards. Significant enhancements have been introduced to the standard with each Wi-Fi generation. While prior amendments such as 802.11a, 11n, and 11ac boosted peak data rates, the 802.11ax amendment prioritizes enhanced capacity, reduced latency, and power efficiency in dense deployments. 802.11ax employs several innovations in the physical (PHY) layer and the medium access control (MAC) layer [2]. These innovations have adopted in the next-generation IEEE 802.11be amendment.

In the PHY layer, 802.11ax has introduced orthogonal frequency division multiple access (OFDMA) in uplink (UL) and downlink (DL), and uplink multi-user multiple-input-multiple-output (MU-MIMO) capabilities. OFDMA improves spectral efficiency by dividing the channel bandwidth into smaller and orthogonal resource units (RUs), which can be allocated to different users based on their data requirements. OFDMA reduces latency and enhances overall user experience by enabling concurrent data transmissions from multiple users to the access point (AP) and vice versa. MU-MIMO improves spectral efficiency by allowing multiple users to transmit over different spatial streams simultaneously on the same RU [3].

In the MAC layer, 802.11ax has introduced a new OFDMA-based hybrid access MAC protocol to enable concurrent uplink transmissions. Hybrid access consists of contention-free scheduled access (SA) and contention-based uplink OFDMA random access (UORA) [4]. The AP controls hybrid access by broadcasting trigger frames (TFs), which contain RU allocation for SA and UORA and scheduling-related information.

In SA, the AP schedules users on the RUs allocated for SA based on their channel conditions. SA has two advantages over UORA. First, the AP can exploit multi-user diversity in SA or implement fairness by employing a suitable scheduler. Second, a user who transmits in SA, which we shall refer to as an SA user, does not face contention-related overheads, such as back-off wait times or wasted transmissions due to collisions. However, UORA is needed because the users provide their buffer status reports (BSRs) to the AP through UORA [4], [5]. UORA employs a variation of the exponential back-off-based distributed coordination function. We refer to users who contend using UORA as UORA users. The user's data rate is adapted to the RU's channel state by an appropriate choice of the modulation and coding scheme (MCS). While the AP selects the MCS in SA, UORA users handle this themselves.

After successfully transmitting its BSR, a UORA user waits for the AP to allocate its SA RUs. It becomes an SA user and no longer participates in the UORA-based contention. Subsequently, after transmitting all the packets reported in its BSR, a user leaves SA. It again becomes a UORA user when it has packets to transmit.

SA improves the overall throughput by allowing contention-free uplink transmissions, while UORA enables users to enter SA and inform the AP about their buffer status. A trade-off exists between the number of RUs allocated to UORA and SA. Intuitively, allocating more RUs to SA increases the contention-free SA throughput. However, this leads to increased contention in UORA due to fewer UORA RUs. The AP might even run out of SA users to schedule if there are fewer successful BSR transmissions through UORA. Furthermore, the average access delay, which is the average time a UORA user spends before it successfully transmits its BSR packet to the AP, increases. Hence, the AP must carefully balance the UORA and SA RU allocation to optimize

S. Arthi and N. B. Mehta are with the Dept. of Electrical Communication Eng. (ECE), Indian Institute of Science (IISc), Bangalore, India (Emails: arthis@iisc.ac.in, nbmehta@iisc.ac.in). C. Singh is with the Dept. of Electronic Systems Eng. (DESE), IISc, Bangalore, India (Email: chandra@iisc.ac.in).

A part of this work has been presented in the IEEE Global Communications Conference (Globecom), Dec. 2024, Cape Town, South Africa [1].

system performance. The RU allocation, the MAC contention protocol, and the time a user stays in SA together affect the aforementioned flow of users between UORA and SA. This trade-off is new compared to previous generations of Wi-Fi, which supported only contention-based uplink transmissions, and cellular networks, where users transmit only when scheduled by the base station.

We now discuss the related literature on 802.11ax.

A. Related Literature on 802.11ax

We classify the related literature on 802.11ax into the following three categories: (i) UORA-focused, (ii) SA-focused, and (iii) hybrid access-focused.

1) UORA-focused: In [6], the uplink saturation throughput is analyzed and an algorithm that tunes the contention parameters to maximize the throughput is proposed. In [7], the average access delay and the access success probability are analyzed. In [8], the uplink saturation throughput is analyzed for multi-basic service set scenarios. In the recent works in [9]–[13], reinforcement learning-based methods and heuristic approaches have been proposed to enhance performance; but they require modifications to the 802.11ax MAC protocol. In [14], back-off mechanisms that captures the joint impact of UORA and multi-link, which is a key feature in Wi-Fi 7 are proposed. However, [6]–[14] do not model SA; UORA is assumed to be the only mechanism for uplink transmissions.

2) SA-focused: In [3], the uplink and downlink saturation throughputs are analyzed for an 802.11ax system that leverages MU-MIMO and OFDMA. In [15], the uplink and downlink saturation throughputs and the head-of-line (HOL) delay are analyzed for two schedulers, one of which maximizes the throughput while the other minimizes the HOL delay. In [16], transmission delay-based user scheduling is proposed for uplink OFDMA. In [17], different scheduling policies, including max-rate, proportional fair, and shortest remaining processing time, are studied for uplink OFDMA. In [18], user scheduling algorithms are proposed for uplink OFDMA and downlink MU-MIMO. In [19], user assignment and user group assignment algorithms are studied using divide-and-conquer-based, greedy, and recursive approaches to maximize the downlink throughput. In [20], a user scheduling policy for downlink OFDMA based on weighted max-min fairness is proposed. In [21], a user scheduling algorithm based on deep hierarchical reinforcement learning is proposed to maximize the throughput. However, [3], [15]–[21] do not model UORA.

3) Hybrid Access-focused: In [4], a hybrid access uplink is considered and the impact of RU allocation on the saturation throughput is analyzed. An algorithm for dynamic RU allocation based on BSR information is proposed. In [5], uplink MU-MIMO and hybrid access are considered, and the saturation throughput and the HOL delay are analyzed. A BSR-based dynamic RU allocation mechanism is also proposed. In [22], a static RU allocation scheme is proposed to minimize a weighted sum of the times required by different users to transmit the HOL packets assuming a fixed number of users in UORA and SA. In [23], the access delay is analyzed when 802.11ax users coexist with legacy users. However, [4], [5], [22], [23] assume that the number of SA users is always equal to the number of SA RUs. This assumption ignores the fact that UORA-based contention determines whether or not a user enters SA. For example, if fewer RUs are allocated for UORA, the average number of SA users will likely be smaller. Furthermore, [4], [5], [22], [23] focus only on the random scheduler.

B. Contributions

To the best of our knowledge, there are no works in the literature that model the IEEE 802.11ax hybrid access MAC protocol along with a dynamic flow of users between UORA and SA. Furthermore, the optimal dynamic policy to allocate RUs for UORA and SA that addresses the fundamental trade-off between saturation throughput and average access delay has not been explored.

For the equal-sized RU configuration, we develop a novel and accurate analysis of the UORA and SA saturation throughputs and the average access delay of hybrid access, which accounts for the dynamic flow of users between UORA and SA. The saturation throughput is an extensively studied performance measure in previous and current generation Wi-Fi systems. It characterizes the system throughput in heavy data traffic conditions [3], [15], [24], [25]. In many wireless systems, it is also the highest throughput that can be achieved by the system. The average access delay is another important performance measure that captures the average waiting time of UORA users to transmit their BSR packets [5], [7], [23].

The analysis then enables us to design a novel dynamic RU allocation policy that adapts the number of RUs allocated for UORA and SA depending on the number of SA users. The analysis also characterizes – for the first time – the saturation throughput and average access delay of static as well as dynamic RU allocation policies. Altogether, this analysis followed by RU allocation policy design addresses a significant gap in the literature, given the relevance of hybrid access and OFDMA to current-generation 802.11ax and next-generation 802.11be Wi-Fi systems.

We make the following contributions:

1) We develop a novel, renewal-theoretic fixed-point analysis of the 802.11ax protocol with hybrid access that leads to accurate expressions for the UORA, SA, and total saturation throughputs and the average access delay for a given allocation of RUs for UORA and SA. Our analysis covers the payload-integrated [4] and time-separated BSR models [5], [23], [26], which have been separately considered in the literature and never compared. It is the first to account for decoding errors and their impact on both UORA and SA. In UORA, a decoding error affects the contention process in a manner similar to a collision since the AP does not send an ACK. Our analysis is also the first to account for the variation in the number of users in UORA and SA over time and its impact on the UORA and SA throughputs. The variation depends on the number of RUs allocated

for UORA and SA, the MAC contention mechanism of 802.11ax, and the time the users spend in SA. We present a novel discrete-time Markov model to characterize this variation, and determine its transition and steady-state probabilities. Our approach differs from [4], [5], [22], [23], which assume a fixed number of users in UORA and SA.

2) Another novel aspect of our approach is its accounting of discrete rate adaption, as specified in the standard, and the AP's scheduler. Our comprehensive analysis covers the random and max-throughput schedulers, which provide different trade-offs between user fairness and SA throughput. This is unlike the literature on hybrid access, which has primarily focused on the random scheduler [4], [5], [22], [23]. While the literature on SA considers channel-aware schedulers, it does not model UORA and its impact on the scheduler and the SA throughput [17]–[20].
3) We employ Markov decision process (MDP) theory to develop an optimal, novel dynamic RU allocation policy (ODRAP) that adapts the number of UORA and SA RUs as a function of the number of SA users. ODRAP maximizes a reward function that is a weighted combination of the saturation throughput and the access delay. It facilitates a trade-off between the saturation throughput and the average access delay. The aforementioned Markov model is central to the development of ODRAP. We design ODRAP for arbitrary, application-specific probability distributions of the number of packets reported in the BSR. We then generalize the above analysis to characterize the saturation throughput and the average access delay of ODRAP and dynamic RU allocation policies, in general. Given its optimality, ODRAP serves as a fundamental benchmark for assessing other RU allocation policies.
4) Our numerical results verify the accuracy of the analytical approach for static and dynamic RU allocation policies, such as BSR-based and ODRAP, despite its simplicity. For static RU allocation, our results reveal that the conventional assumption in [4], [5] of a fixed number of UORA and SA users leads to incorrect estimates of the UORA and SA saturation throughputs. Our results also bring out, for the first time, the dependence of the max-throughput scheduler's throughput on the number of RUs allocated to UORA. ODRAP achieves a higher reward than all benchmark RU allocation policies for any number of users served by the wireless local area network (WLAN). Our results reveal that ODRAP optimally trades off between the saturation throughput and the average access delay, unlike the BSR-based policy which tries to improve the saturation throughput, and the delay-focused policy, which tries to reduce the average access delay.

Table I summarizes the key differences between our work and the literature. Unlike most works on 802.11ax [3], [6]–[8], [13], [15]–[21] that focus on either UORA or SA, our model considers both. While [4], [5], [22], [23] model UORA and SA, they do not consider the dynamic flow of users between the two. While [15], [17]–[21] consider a channel-aware scheduler, they do not analyze the scheduler's throughput. While [18]–[20] model the discrete-rate adaptation, only the simulation results are presented. An accurate analysis and comparison of the payload-integrated and time-separated BSR models is not available in the literature. The impact of decoding errors on UORA and SA has also not been studied in the literature. Our work differs from the conventional 802.11 MAC analyzes [24], [25], which do not consider SA, do not have multiple RUs to transmit in UORA, and follow a different rule for decrementing the back-off counter.

TABLE I
COMPARISON OF RELATED LITERATURE ON IEEE 802.11AX

Reference	UORA	SA	Scheduler	Decoding errors	Discrete rate adaptation	RU allocation
[6]–[14]	Yes	No	No	No	No	- NA -
[3]	No	UL	Random	No	No	- NA -
[15], [17]	No	UL	1. Max throughput 2. Min HOL delay	No	No	- NA -
[16]	No	UL	Transmission delay	No	No	- NA -
[21]	No	UL	Max throughput	No	No	- NA -
[18]	No	UL	Max throughput	No	Yes	- NA -
[19], [20]	No	DL	Max throughput	No	Yes	- NA -
[4], [5]	Yes	UL	Random	No	No	1. Static 2. Dynamic (BSR-based)
[22]	Yes	UL	Random	No	No	Static (minimize HOL delay)
[23]	Yes	UL	Random	No	No	Static
This manuscript	Yes	UL	1. Max throughput 2. Random	Yes	Yes	1. Static 2. Dynamic (general) 3. Optimal

C. Outline and Notations

We present the system model in Section II. We analyze the saturation throughput in Section III. We design the optimal dynamic RU allocation policy in Section IV. Section V presents numerical results, and Section VI contains our conclusions.

Notations: $\mathbb{1}_{\{a\}}$ denotes the indicator function; it is 1 if a is true and is 0 otherwise; $\lceil \cdot \rceil$ denotes the ceiling function; and x^+ denotes $\max\{x, 0\}$. The probability of an event A is denoted by $\Pr(A)$, and the conditional probability of A given B is denoted by $\Pr(A|B)$. The expectation of a random variable X is denoted by $\mathbb{E}[X]$, and the conditional expectation of X given Y is denoted by $\mathbb{E}[X|Y]$. The multinomial coefficient is defined as $\binom{n}{k_1,k_2,\ldots,k_m} := \frac{n!}{k_1!k_2!\ldots k_m!}$ for $k_1, \ldots, k_m \geq 0$ and $k_1 + \cdots + k_m = n$. Appendix A tabulates the other notations used in this paper.

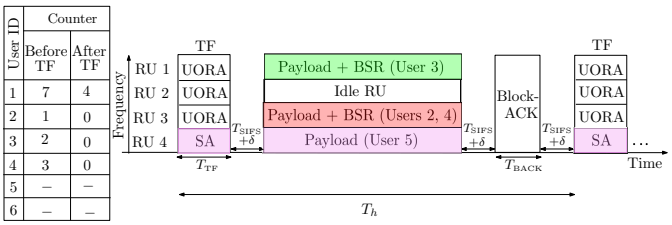

Fig. 1. Illustration of hybrid access in IEEE 802.11ax with two SA and four UORA users, where one RU is allocated for SA and three RUs for UORA.

II. SYSTEM MODEL

We consider an uplink 802.11ax system with an AP and K users. All the users support hybrid access. Each user can sense transmissions from the other users, as is typical in a dense deployment. The channel bandwidth is divided into N_{RU} equal-sized RUs. Of these, N_{RA} RUs are allocated for UORA and $N_{\text{SA}} = N_{\text{RU}} - N_{\text{RA}}$ RUs are allocated for SA.

Equal-sized RUs is one of the RU configurations specified in the IEEE 802.11ax standard. It is also the most widely studied configuration due to its tractability [4], [5], [15]. We also focus on the equal-sized RU configuration given its theoretical and practical relevance. Our approach can be extended to handle unequal RU sizes, but at the expense of more involved bookkeeping. In addition to tracking the number of UORA and SA users, we would also need to track the RUs each of them occupies as the RU sizes are different.

A. Hybrid Access in 802.11ax

The AP manages hybrid access by transmitting a trigger frame (TF) every T_h sec. The AP has a higher priority to access the channel frequently and initiate hybrid access. This is achieved by using enhanced distributed channel access (EDCA), which configures the AP with smaller arbitration inter-frame spacing and contention window values. Modeling the impact of legacy users, which do not use 802.11ax, is beyond the scope of this work. We shall refer to the duration between two successive TFs as a TF cycle. A TF contains N_{RA}, the list of users scheduled using SA, and their user-specific information, which includes RU and spatial stream allocation, MCSs, coding types, and target powers [27, subcl. 9.3.1.22.1]. Here, the coding type indicates whether a low-density parity check (LDPC) code or a binary convolutional code was used as the channel code for the user's data packet.

At any instant of time, a user is either a UORA or an SA user. Each UORA user uniformly samples its back-off counter from the set $\{1, 2, \ldots, C\}$, where C denotes the OFDMA contention window. After receiving a TF, a UORA user decrements its back-off counter by N_{RA}, thereby implementing bulk back-off decrements, and resets it to 0 if it becomes negative. When the back-off counter becomes zero, the UORA user transmits a data packet along with its BSR on a randomly chosen UORA RU after a short inter-frame spacing (SIFS) of duration T_{SIFS}. This transmission is successful if no other UORA user transmits on the same RU and the packet is decoded successfully. In this case, the user resets C to $C_{\min}$. Otherwise, a collision occurs and the user doubles C unless C equals $C_{\max}$. A user that has collided i times is said to be at back-off stage $\min\{i, \rho\}$ where $\rho = \log_2(C_{\max}/C_{\min})$. Hence, the contention window C_i at the back-off stage i is $2^i C_{\min}$. We do not impose a cap on the number of re-transmissions.

The AP schedules each SA user until the user transmits all the packets reported in its BSR. Each SA user transmits a data packet on its allocated RU without contention. Therefore, the SA transmissions are successful except when a packet loss occurs due to decoding errors. This happens with probability ε which is the target PER. The SA transmissions do not include BSRs, which is consistent with the hybrid access models of [4], [5], [22]. After T_{SIFS}, the AP acknowledges all the successful transmissions by either sending acknowledgments (ACKs) on the same RUs in which it has received the packets or by broadcasting a block-ACK to all the users, which occupies the entire bandwidth. We refer to this transmission model as the *payload-integrated BSR model*.

Fig. 1 illustrates hybrid access with four UORA users, numbered 1, 2, 3, and 4, and two SA users, numbered 5 and 6. RUs 1, 2, and 3 are allocated for UORA, and RU 4 is allocated for SA. The AP schedules the SA user 5 on RU 4, while SA user 6 waits for its turn in the subsequent TF cycles. Since $N_{\text{RA}} = 3$, the back-off counters of users 2, 3, and 4 get decremented to 0, and they choose to transmit on RUs 3, 1, and 3, respectively. Thus, a successful transmission by user 3 occurs on RU 1, a collision between users 2 and 4 occurs on RU 3, and no transmission occurs on RU 2. The AP sends a block-ACK after T_{SIFS} sec.

Time-separated BSR Model: Our analytical framework also covers the time-separated BSR model, which has been considered in [5], [23], [26]. In this alternate model, hybrid access consists of two steps. In the first step, the AP transmits a TF and initiates UORA. After T_{SIFS} duration, the UORA users contend to transmit the BSR packets on UORA RUs while the SA RUs remain idle. In the second step, the AP again transmits a TF to acknowledge the successful BSR transmissions and schedules the SA users. The SA users or a subset of them transmit on SA RUs, while UORA RUs remain unutilized. We present illustrative flowcharts for these two models in Appendix B.

B. Channel Model and Discrete Rate Adaptation

We consider the general Nakagami-m fading model. It models line-of-sight (LoS) and non-LoS channels, which arise in indoor environments [28], [29], and includes as special cases Rayleigh fading ($m = 1$) and transmit-receive diversity. Let $g_{u,r}$ denote the power of the uplink small-scale fading gain of user u on RU r. Without loss of generality, $\mathbb{E}[g_{u,r}] = 1$. Since the square of a Nakagami-m random variable follows the gamma distribution, the PDF of $g_{u,r}$ is [28, Ch. 3]

$$f(x) = \frac{m^m x^{m-1}}{\Gamma(m)} \exp(-mx), \quad \text{for } x \geq 0, \tag{1}$$

where m is the shape parameter.

TABLE II
THROUGHPUTS AND SNR THRESHOLDS FOR MCSS SPECIFIED IN IEEE 802.11AX ($\varepsilon = 0.1$)

Index (τ)	Modulation	Code rate	Throughput r_τ in Mbps	SNR threshold Υ_τ in dB
1	BPSK	1/2	3.18	-0.65
2	QPSK	1/2	6.37	2.35
3	QPSK	3/4	9.56	4.81
4	16-QAM	1/2	12.75	7.89
5	16-QAM	3/4	19.12	10.90
6	64-QAM	2/3	25.50	15.09
7	64-QAM	3/4	28.68	16.46
8	64-QAM	5/6	31.87	18.00
9	256-QAM	3/4	38.25	21.65
10	256-QAM	5/6	42.50	23.46
11	1024-QAM	3/4	47.81	26.78
12	1024-QAM	5/6	53.12	28.85

Let σ^2 denote the noise variance and P_{rx} denote the fading-averaged received power at the AP on an RU. Then, $P_{\text{rx}} = P_{\text{tx}} \left(\frac{c}{4\pi d_0 f_c}\right)^2 \left(\frac{d_0}{d}\right)^\eta$, where P_{tx} is the transmit power, d is the distance between user u and the AP, η is the path-loss exponent, $d_0 \leq d$ is the critical distance, c is the speed of light, and f_c is the carrier frequency [28, Ch. 2.6]. Hence, the signal-to-noise ratio (SNR) of user u on RU r is $\frac{P_{\text{rx}} g_{u,r}}{\sigma^2}$. To model the different distances users can be from the AP, we distributed them uniformly in an annular region of inner radius L and outer radius D centered at the AP. Other user location models can also be incorporated in our framework.

Let $\Delta = \{0, 1, \ldots, M\}$ denote the set of MCS indices and let r_τ be the throughput of MCS τ. Let Υ_τ be the smallest SNR at which the packet error rate (PER) of MCS τ equals the target value of ε. Typically, ε is set as 0.1. Thus, a user transmits with MCS τ if its SNR falls between Υ_τ and $\Upsilon_{\tau+1}$. MCS 0 corresponds to no-transmission ($r_0 = 0$), which happens when the SNR is below Υ_1. Table II lists the constellation and LDPC code rate for each MCS specified in IEEE 802.11ax, and its throughput and SNR threshold. The throughputs are for an RU with 102 data subcarriers and a single spatial stream.[1] In 802.11ax, the OFDM symbol duration in a payload frame is 16 μs [3]. The thresholds are available in ns-3 [30]. We see that there are $M = 12$ MCSs with throughputs varying from 3.18 Mbps for MCS 1 to 53.12 Mbps for MCS 12.

C. User Scheduling in 802.11ax

Let k_{sa} denote the number of SA users and $k_{\text{ra}} = K - k_{\text{sa}}$ denote the number of UORA users. Let $\mathcal{B}$ be the set of SA users and $\mathcal{D}$ be the set of SA RUs. A scheduler's assignment is defined by the set $\mathcal{V} = \{x_{u,r}, \forall u \in \mathcal{B}, r \in \mathcal{D}\}$, where $x_{u,r}$ is 1 if user u is allocated to RU r, and is 0 otherwise. The assignment must satisfy two 802.11ax-specific constraints: (1) each RU is assigned to at most one user, and (2) each user is assigned to at most one RU.

[1]The extension to single-user MIMO, where a user can have multiple spatial streams in an RU, is straightforward and only changes the throughput. However, the scheduler design in Section II-C needs to be revisited for MU-MIMO, where more than one user can be scheduled in an RU.

We consider the following two schedulers, which provide different trade-offs between fairness and SA throughput:

1) *Random Scheduler [4], [5]:* This scheduler randomly allocates the SA RUs to the SA users. It is fair in the sense that each SA user has an equal probability of being scheduled in a TF cycle. In this scheduler, $\mathcal{V}$ is a set of 0's and 1's that satisfy the 802.11ax-specific constraints.
2) *Max-throughput Scheduler [18]:* This scheduler sacrifices fairness for higher throughput. It solves the following constrained optimization problem to maximize the sum throughput:

$$\mathcal{J}: \max_{x_{u,r}, \forall u \in \mathcal{B}, r \in \mathcal{D}} \left\{ \sum_{u \in \mathcal{B}} \sum_{r \in \mathcal{D}} x_{u,r} R_{u,r} \right\}, \tag{2}$$

$$\text{s.t.} \sum_{u \in \mathcal{B}} x_{u,r} \leq 1, \ \forall r \in \mathcal{D}, \tag{3}$$

$$\sum_{r \in \mathcal{D}} x_{u,r} \leq 1, \ \forall u \in \mathcal{B}, \tag{4}$$

$$x_{u,r} \in \{0, 1\}, \ \forall u \in \mathcal{B}, r \in \mathcal{D}. \tag{5}$$

Here, $R_{u,r}$ is the throughput of user u on RU r; it depends on the MCS chosen, which is a function of the SNR of user u on RU r. The AP can know this SNR through a channel-sounding procedure. The AP sends the beamforming report poll TF to the SA users and requests channel state information (CSI); then, the SA users transmit their CSI reports to the AP on the allocated RUs. Constraints (3) and (4) are 802.11ax-specific constraints. The solution to $\mathcal{J}$ is $\mathcal{V}$. This optimization problem can be solved using the Kuhn-Munkres algorithm, which has a polynomial-time complexity of $O((k_{\text{sa}} + N_{\text{SA}})^3)$ [31, Ch. 3].

D. RU Allocation Policies

Let $\mathcal{K} = \{0, 1, \ldots, K\}$ and $\mathcal{R} = \{0, 1, \ldots, N_{\text{RU}}\}$. An RU allocation policy $\pi : \mathcal{K} \to \mathcal{R}$ maps the number of SA users $k_{\text{sa}} \in \mathcal{K}$ to a corresponding number of UORA RUs $N_{\text{RA}} = \pi(k_{\text{sa}}) \in \mathcal{R}$. The following are examples of π:

1) *Static RU Allocation Policy [4], [5], [23]:* Here, the AP allocates a fixed number $n \in \mathcal{R}$ of RUs to UORA. Hence, $\pi(k_{\text{sa}}) = n, \forall k_{\text{sa}} \in \mathcal{K}$.
2) *BSR-based RU Allocation Policy [4], [5]:* Here, the AP allocates just enough RUs for SA to schedule all the SA users (whose BSRs are known to the AP). Hence, $N_{\text{SA}} = \min\{k_{\text{sa}}, N_{\text{RU}}\}$ and $\pi(k_{\text{sa}}) = N_{\text{RU}} - N_{\text{SA}} = (N_{\text{RU}} - k_{\text{sa}})^+, \forall k_{\text{sa}} \in \mathcal{K}$.

III. ANALYSIS: SATURATION THROUGHPUT AND AVERAGE ACCESS DELAY

We first analyze the saturation throughput and the average access delay of static RU allocation policies. We analyze dynamic RU allocation policies in Section IV-C.

The back-off processes of the UORA users are coupled. They are exactly modeled by a discrete-time Markov chain (DTMC) [32]. The state of this DTMC in TF cycle t is the

vector $\mathbf{M}(t) = (M_0(t), M_1(t), \ldots, M_\rho(t))$, where $M_i(t)$ is the number of users in back-off stage i in TF cycle t. The process $\mathbf{M}(t), t \geq 0$, is an irreducible and aperiodic Markov chain on the state space $\mathcal{M} = \{\mathbf{m} = (m_0, m_1, \ldots, m_\rho) \in \mathbb{Z}^{\rho+1} : \sum_{i=0}^{\rho} m_i = K\}$. However, the number of states is $O(K^\rho)$. This large number of states makes an exact analysis intractable even for small K.

We employ the following two decoupling approximations, initially proposed in [25], to develop a simple, yet accurate analysis of hybrid access:

- The back-off process of a given UORA user is independent of the aggregate attempt process of all the other UORA users.
- Each attempt by a UORA user collides with a probability that is independent of its back-off stage.

The decoupling approximations have been widely used in the Wi-Fi and 802.11ax literature; see [4], [5], [24], [25] and the references therein. The theoretical justification for these approximations is provided by mean field theory [33]. The results in [24], [32] show that the decoupling approximations are accurate even for a relatively small number of users. We also confirm the accuracy of these approximations for the hybrid access MAC in Section V. Based on these approximations, we define the following UORA back-off parameters.

1) *Attempt Rate* $\beta(k_{ra})$*:* Each UORA user attempts a transmission in a TF cycle with probability $\beta(k_{\text{ra}})$. Formally, $\beta(k_{\text{ra}}) = \Pr(\text{a UORA user attempts to transmit in a TF cycle})$.
2) *Conditional Collision Probability* $\alpha(k_{ra})$*:* Conditioned on a UORA user transmitting, its transmission suffers a collision with probability $\alpha(k_{\text{ra}})$. Formally, $\alpha(k_{\text{ra}}) = \Pr(\text{the packet transmitted by UORA user } i \text{ collides} \mid \text{UORA user } i \text{ transmits})$.

Since we focus on the saturation throughput, each user always has a packet to transmit. The outline of our analysis is as follows. We derive expressions for $\alpha(k_{\text{ra}})$ and $\beta(k_{\text{ra}})$ in Section III-A assuming that the system is in a steady state with k_{ra} users in UORA. Then, we present a Markov model for the evolution of k_{ra} and obtain the steady-state probabilities of k_{ra} and k_{sa} in Section III-B. In Section III-C, we compute the UORA and SA saturation throughputs in Results 2 and 3 as a function of k_{ra} and k_{sa}, and average them using the steady-state probabilities.

A. Renewal-theoretic Analysis of UORA

We now derive expressions for $\alpha(k_{\text{ra}})$ and $\beta(k_{\text{ra}})$.

1) Conditional Collision Probability: When a UORA user transmits on a particular UORA RU with probability $\frac{\beta(k_{\text{ra}})}{N_{\text{RA}}}$, a collision occurs if at least one among the other $k_{\text{ra}}-1$ UORA users also transmits on the same RU. Hence,

$$\alpha(k_{\text{ra}}) = 1 - \left(1 - \frac{\beta(k_{\text{ra}})}{N_{\text{RA}}}\right)^{k_{\text{ra}}-1}, \quad \forall 1 \leq k_{\text{ra}} \leq K. \tag{6}$$

2) Attempt Rate: For a UORA user, let b_i denote the mean back-off duration in TF cycles for the i^{th} attempt.

Lemma *1:* For $N_{\text{RA}} \leq C_i$, we have

$$b_i = \begin{cases} \left\lceil \frac{C_i}{N_{\text{RA}}} \right\rceil \left(1 - \left(\left\lceil \frac{C_i}{N_{\text{RA}}} \right\rceil - 1\right) \frac{N_{\text{RA}}}{2C_i}\right), & \forall 0 \leq i \leq \rho - 1, \\ \left\lceil \frac{C_{\max}}{N_{\text{RA}}} \right\rceil \left(1 - \left(\left\lceil \frac{C_{\max}}{N_{\text{RA}}} \right\rceil - 1\right) \frac{N_{\text{RA}}}{2C_{\max}}\right), & \forall i \geq \rho. \end{cases} \tag{7}$$

For $N_{\text{RA}} > C_i$, $b_i = 1$.

Proof: We first derive b_i when $N_{\text{RA}} \leq C_i$. For an arbitrary UORA user, let w_i, $\forall i \geq 0$, denote the OFDMA back-off counter, and let $B_j^{(i)}$, $\forall i \geq 0$, $j \geq 1$, denote the back-off duration in TF cycles for the i^{th} attempt of its j^{th} BSR packet. Since w_i is uniformly sampled from the set $\{1, 2, \ldots, C_i\}$ and is decremented by N_{RA} in each TF cycle, we have $\Pr(B_j^{(i)} = n) = \Pr\left((n-1)N_{\text{RA}} < w_i \leq nN_{\text{RA}}\right) = \frac{N_{\text{RA}}}{C_i}$, $\forall 1 \leq n \leq \left\lceil \frac{C_i}{N_{\text{RA}}} \right\rceil - 1$. It follows that

$$\Pr\left(B_j^{(i)} = \left\lceil \frac{C_i}{N_{\text{RA}}} \right\rceil\right) = 1 - \sum_{n=1}^{\left\lceil \frac{C_i}{N_{\text{RA}}} \right\rceil - 1} \Pr(B_j^{(i)} = n), \tag{8}$$

$$= 1 - \frac{N_{\text{RA}}}{C_i}\left(\left\lceil \frac{C_i}{N_{\text{RA}}} \right\rceil - 1\right). \tag{9}$$

We can then show that

$$b_i = \mathbb{E}\left[B_j^{(i)}\right] = \sum_{n=1}^{\left\lceil \frac{C_i}{N_{\text{RA}}} \right\rceil} n \Pr(B_j^{(i)} = n), \tag{10}$$

$$= \left\lceil \frac{C_i}{N_{\text{RA}}} \right\rceil \left(1 - \left(\left\lceil \frac{C_i}{N_{\text{RA}}} \right\rceil - 1\right) \frac{N_{\text{RA}}}{2C_i}\right). \tag{11}$$

Similarly, since $C_i = C_{\max}$, $\forall i \geq \rho$, we can show that $b_i = \left\lceil \frac{C_{\max}}{N_{\text{RA}}} \right\rceil \left(1 - \left(\left\lceil \frac{C_{\max}}{N_{\text{RA}}} \right\rceil - 1\right) \frac{N_{\text{RA}}}{2C_{\max}}\right)$, $\forall i \geq \rho$.

When $N_{\text{RA}} > C_i$, we have $\Pr(B_j^{(i)} = 1) = 1$, since one TF cycle is enough for the back-off counter to be decremented to 0. Hence, $b_i = 1$. ∎

In typical IEEE 802.11ax configurations, C_i ranges from 16 to 1024 depending on the back-off stage. N_{RA} ranges from 1 to 74 when 26-tone RUs are used in a 160 MHz channel. It is even lower for other RU configurations. Hence, in these settings $C_i/N_{\text{RA}} \gg 1$. When $C_i/N_{\text{RA}} \gg 1$, $\left\lceil \frac{C_i}{N_{\text{RA}}} \right\rceil \approx \frac{C_i}{N_{\text{RA}}} + 1$, and (7) simplifies to

$$b_i = \begin{cases} \frac{1}{2}\left(\frac{C_i}{N_{\text{RA}}} + 1\right), & \forall 0 \leq i \leq \rho - 1, \\ \frac{1}{2}\left(\frac{C_{\max}}{N_{\text{RA}}} + 1\right), & \forall i \geq \rho. \end{cases} \tag{12}$$

Result *1:* For $N_{\text{RA}} \leq C_i$, the attempt rate of a UORA user is given by

$$\beta(k_{\text{ra}}) = \frac{2N_{\text{RA}}(1 - 2\gamma(k_{\text{ra}}))}{\left[\begin{array}{l}(1 - 2\gamma(k_{\text{ra}}))(C_{\min} + N_{\text{RA}}) \\ +\gamma(k_{\text{ra}})C_{\min}\left(1 - 2^\rho\gamma^\rho(k_{\text{ra}})\right)\end{array}\right]} \tag{13}$$

where

$$\gamma(k_{\text{ra}}) = \alpha(k_{\text{ra}}) + (1 - \alpha(k_{\text{ra}}))\varepsilon, \tag{14}$$

is the probability that a UORA packet is not successfully decoded by the AP. For $N_{\text{RA}} > C_i$, we have $\beta(k_{\text{ra}}) = 1, \forall 1 \leq k_{\text{ra}} \leq K$.

Proof: We modify the renewal-theoretic approach in [24] to account for the OFDMA-based MAC contention and bulk back-off decrements. For an arbitrary UORA user, let A_j denote the number of transmission attempts of its j^{th} BSR packet, $\forall j \geq 1$. The total back-off duration H_j is equal to

$$H_j = \sum_{i=0}^{A_j-1} B_j^{(i)}. \tag{15}$$

From the decoupling approximations, $H_j, \forall j \geq 1$, form a sequence of renewal cycles. The start of the 0^{th} back-off counter decrement for transmitting a BSR constitutes a renewal instant. We define the reward in the j^{th} renewal cycle as A_j. From the renewal reward theorem [34, Ch. 5.4], we get

$$\beta(k_{\text{ra}}) = \frac{\mathbb{E}[A_j]}{\mathbb{E}[H_j]}. \tag{16}$$

a) Derivation of $\mathbb{E}[A_j]$*:* From the decoupling approximations, it follows that $\Pr(A_j = n) = \gamma^{n-1}(k_{\text{ra}})(1-\gamma(k_{\text{ra}}))$, $\forall n \geq 1$. Hence,

$$\mathbb{E}[A_j] = \sum_{n=1}^{\infty} n \Pr(A_j = n) = \frac{1}{1-\gamma(k_{\text{ra}})}. \tag{17}$$

b) Derivation of $\mathbb{E}[H_j]$*:* Using the law of total expectation, $\mathbb{E}[H_j] = \sum_{n=1}^{\infty} \Pr(A_j = n)\mathbb{E}[H_j | A_j = n]$. Further, we have $\mathbb{E}[H_j | A_j = n] = \sum_{i=0}^{n-1} \mathbb{E}\left[B_j^{(i)}\right] = b_0 + \cdots + b_{n-1}$. Simplifying further, we get

$$\mathbb{E}[H_j] = \sum_{n=1}^{\infty} (b_0 + \cdots + b_{n-1}) \Pr(A_j = n), \tag{18}$$

$$= b_0 + \gamma(k_{\text{ra}}) b_1 + \gamma^2(k_{\text{ra}}) b_2 + \cdots. \tag{19}$$

Substituting (17), (19), and b_i from (12) in (16) and simplifying further yields (13) for $N_{\text{RA}} \leq C_i$. Similarly, substituting $b_i = 1$ yields $\beta(k_{\text{ra}}) = 1$ for $N_{\text{RA}} > C_i$. ∎

Since (6) and (13) are continuous mappings from $[0,1]$ to $[0,1]$, a fixed-point exists in $[0,1]$ by Brouwer's fixed-point theorem. The fixed-point can be shown to be unique since $b_0, b_1, \ldots$ is a non-decreasing sequence [24, Thm. 5.1]. We solve (6) and (13) numerically for each value of k_{ra}.

Note: The above expressions differ from those in the legacy 802.11 MAC literature [24], [25] as the OFDMA-based UORA contention employed in 802.11ax is different from the mechanism in legacy WLANs. Our results are consistent with the expressions obtained in [4]. However, a key distinction in our work is that (6) and (13) are functions of k_{ra}, which is a random variable and can change with time. This alters the analysis that follows below.

B. Evolution of the Number of Users in SA and UORA

We model the number of packets reported in a BSR as a random variable. Thus, the number reported by a user can vary from one BSR to another. In general, the probability distribution of the number of reported packets depends on the application. We first consider the case where the number of packets reported in a user's BSR is geometrically distributed with mean $s \geq 1$, which we shall refer to as the geometric buffer distribution. We extend our approach to general distributions in Section IV-D. Each SA user stays in SA until it transmits all the packets reported in its BSR. The number of TF cycles a user stays in SA depends not just on the number of packets reported in its BSR, but also the number of SA RUs and the scheduler.[2] This is because an SA user might not be scheduled to transmit in every TF cycle if there are more SA users than the number of RUs allocated for SA.

The state of the system is the number of SA users $X(t)$ in TF cycle t. Furthermore, $X(t) \in \{0, 1, \ldots, K\}$. The decoupling approximations and the memory-less property of the geometric distribution imply that the process $X(t), t \geq 1$, is a DTMC.

To compute the steady-state probabilities of the DTMC, we first determine the probability $\zeta_n^{(k_{\text{ra}})}$ of the event that n out of k_{ra} UORA users successfully transmit their BSR packets.

Lemma *2:* Let $\boldsymbol{x} = (x_1, \ldots, x_{N_{\text{RA}}})$ and $\boldsymbol{\ell} = (l_1, \ldots, l_{N_{\text{RA}}})$. Let $\Omega(k_{\text{ra}})$ represent the set of all N_{RA}-length vectors whose elements belong to the set $\{0, 1, \ldots, k_{\text{ra}}\}$. Consider the polynomial

$$f_{k_{\text{ra}}}(\boldsymbol{x}) = \left(\frac{\beta(k_{\text{ra}})}{N_{\text{RA}}} \sum_{j=1}^{N_{\text{RA}}} [\varepsilon x_j + (1-\varepsilon)x_j] + 1 - \beta(k_{\text{ra}}) \right)^{k_{\text{ra}}},$$

$$= \sum_{i=0}^{k_{\text{ra}}} \frac{\phi_i(k_{\text{ra}})}{N_{\text{RA}}^i} \sum_{\boldsymbol{\ell} \in \Omega(k_{\text{ra}})} \mathbb{1}_{\left\{\sum_{j=1}^{N_{\text{RA}}} l_j = i\right\}} \binom{i}{l_1, \ldots, l_{N_{\text{RA}}}} \times \prod_{j=1}^{N_{\text{RA}}} [\varepsilon x_j + (1-\varepsilon)x_j]^{l_j}, \tag{20}$$

where $\phi_i(k_{\text{ra}}) = \binom{k_{\text{ra}}}{i} (\beta(k_{\text{ra}}))^i (1-\beta(k_{\text{ra}}))^{k_{\text{ra}}-i}$. Let $v(\boldsymbol{\ell}) = \sum_{j=1}^{N_{\text{RA}}} \mathbb{1}_{\{l_j = 1\}}$. Then, for all $0 \leq n \leq \min\{k_{\text{ra}}, N_{\text{RA}}\}$, we have

$$\zeta_n^{(k_{\text{ra}})} = \sum_{i=0}^{k_{\text{ra}}} \frac{\phi_i(k_{\text{ra}})}{N_{\text{RA}}^i} \sum_{\boldsymbol{\ell} \in \Omega(k_{\text{ra}})} \binom{i}{l_1, \ldots, l_{N_{\text{RA}}}} \binom{v(\boldsymbol{\ell})}{n} \times \mathbb{1}_{\left\{\sum_{j=1}^{N_{\text{RA}}} l_j = i\right\}} \mathbb{1}_{\{v(\boldsymbol{\ell}) \geq n\}} (1-\varepsilon)^n \varepsilon^{v(\boldsymbol{\ell})-n}. \tag{21}$$

Proof: Since each UORA user attempts to transmit with probability $\beta(k_{\text{ra}})$, the probability $\phi_i(k_{\text{ra}})$ that i out of k_{ra} UORA users attempt to transmit is given by

$$\phi_i(k_{\text{ra}}) = \binom{k_{\text{ra}}}{i} (\beta(k_{\text{ra}}))^i (1-\beta(k_{\text{ra}}))^{k_{\text{ra}}-i}. \tag{22}$$

Furthermore, the probability that a UORA user transmits on a given UORA RU is $\frac{\beta(k_{\text{ra}})}{N_{\text{RA}}}$.

Let $l_j, \forall 1 \leq j \leq N_{\text{RA}}$, denote the number of UORA users that transmit on the j^{th} UORA RU. The occurrence of the term $x_j^{l_j}$ in the expansion of $f_{k_{\text{ra}}}(\boldsymbol{x})$ implies that l_j users transmitted on the j^{th} UORA RU. When $i = \sum_{j=1}^{N_{\text{RA}}} l_j$

[2]Given our focus on saturation throughput, we assume that the payload of the packet transmitted is a function of the MCS. In practice, aggregation and segmentation are used to deal with variabilities in the packet payload and the data rates.

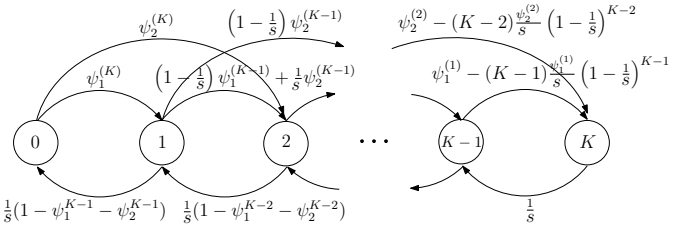

Fig. 2. Illustration of the discrete-time Markov chain model for the evolution of k_{sa} for $N_{\text{RA}}=2$ and $N_{\text{SA}}=1$.

UORA users attempt to transmit, n of them succeed if $n+m$ UORA users transmit on distinct UORA RUs and n of these are successfully decoded without errors. Here, $0\le i\le k_{\text{ra}}$, $0\le n\le \min\{i,N_{\text{RA}}\}$, and $0\le m\le \min\{i,N_{\text{RA}}\}-n$. The probability of this event is given by the coefficient of $x_1^{l_1}x_2^{l_2}\dots x_{N_{\text{RA}}}^{l_{N_{\text{RA}}}}$ in the expansion of $f_{k_{\text{ra}}}(\boldsymbol{x})$ when $\sum_{j=1}^{N_{\text{RA}}} l_j=i$, $\sum_{j=1}^{N_{\text{RA}}}\mathbb{1}_{\{l_j=1\}}\ge n$, and the exponent of the term $1-\varepsilon$ is equal to n. Therefore, it is equal to

$$\frac{\phi_i(k_{\text{ra}})}{N_{\text{RA}}^i}\sum_{\boldsymbol{\ell}\in\Omega(k_{\text{ra}})}\binom{i}{l_1,\dots,l_{N_{\text{RA}}}}\binom{v(\boldsymbol{\ell})}{n}(1-\varepsilon)^n\varepsilon^{v(\boldsymbol{\ell})-n}\times\mathbb{1}_{\left\{\sum_{j=1}^{N_{\text{RA}}}l_j=i\right\}}\mathbb{1}_{\{v(\boldsymbol{\ell})\ge n\}},$$

where $v(\boldsymbol{\ell})=\sum_{j=1}^{N_{\text{RA}}}\mathbb{1}_{\{l_j=1\}}$. Here, the indicator function $\mathbb{1}_{\left\{\sum_{j=1}^{N_{\text{RA}}}l_j=i\right\}}$ ensures that exactly i UORA users attempt to transmit, and $\mathbb{1}_{\{v(\boldsymbol{\ell})\ge n\}}$ ensures that at least n users attempt on distinct UORA RUs. Summing this probability over all i yields (21). ∎

As k_{ra} increases, the cardinality of the set $\Omega(k_{\text{ra}})$ grows exponentially. This increases the complexity of calculating $\zeta_n^{(k_{\text{ra}})}$. The following iterative update addresses this problem. Let $\psi_i(k_{\text{ra}},n)=\sum_{\boldsymbol{\ell}\in\Omega(k_{\text{ra}})}\binom{i}{l_1,\dots,l_{N_{\text{RA}}}}\binom{v(\boldsymbol{\ell})}{n}\mathbb{1}_{\left\{\sum_{j=1}^{N_{\text{RA}}}l_j=i\right\}}\mathbb{1}_{\{v(\boldsymbol{\ell})\ge n\}}(1-\varepsilon)^n\varepsilon^{v(\boldsymbol{\ell})-n}$ denote the inner summand in (21). Then, we can show that

$$\psi_i(k_{\text{ra}},n)=\psi_i(k_{\text{ra}}-1,n)+\sum_{\boldsymbol{\ell}\in\Omega(k_{\text{ra}})\setminus\Omega(k_{\text{ra}}-1)}\binom{i}{l_1,\dots,l_{N_{\text{RA}}}}\times\mathbb{1}_{\left\{\sum_{j=1}^{N_{\text{RA}}}l_j=i\right\}}\mathbb{1}_{\{v(\boldsymbol{\ell})\ge n\}}(1-\varepsilon)^n\varepsilon^{v(\boldsymbol{\ell})-n}. \quad (23)$$

Thus, $\psi_i(k_{\text{ra}},n)$ can be determined from the calculations done for smaller values of k_{ra}. Furthermore,

$$\zeta_n^{(k_{\text{ra}})}=\sum_{i=0}^{k_{\text{ra}}}\frac{\phi_i(k_{\text{ra}})}{N_{\text{RA}}^i}\psi_i(k_{\text{ra}}-1,n)+\sum_{i=0}^{k_{\text{ra}}}\frac{\phi_i(k_{\text{ra}})}{N_{\text{RA}}^i}\sum_{\boldsymbol{\ell}\in\Omega(k_{\text{ra}})\setminus\Omega(k_{\text{ra}}-1)}\mathbb{1}_{\left\{\sum_{j=1}^{N_{\text{RA}}}l_j=i\right\}}\mathbb{1}_{\{v(\boldsymbol{\ell})\ge n\}}(1-\varepsilon)^n\varepsilon^{v(\boldsymbol{\ell})-n}\binom{i}{l_1,\dots,l_{N_{\text{RA}}}}. \quad (24)$$

Transition Probabilities: Let

$$p_{ij}=\Pr\left(X(t+1)=j|X(t)=i\right). \quad (25)$$

We first specify p_{ij} for $i\ne j$.

1) *When $X(t)=0$: k_{sa}* increases to j if j UORA transmissions succeed. Here, $j\le\min\{N_{\text{RA}},K\}$ because $k_{\text{sa}}\le K$ and no more than N_{RA} UORA transmissions can succeed in a TF cycle. This event occurs with probability $\zeta_j^{(K)}$. Thus,
$$p_{ij}=\zeta_j^{(K)},\ \forall i=0 \text{ and } 1\le j\le\min\{N_{\text{RA}},K\}. \quad (26)$$
2) *When $X(t)=i$ and $j>i$: k_{sa}* increases from i to j if $j-i+n$ UORA transmissions succeed and n SA users depart, where $n\in\{0,1,\dots,\min\{N_{\text{SA}},i,K-j,N_{\text{RA}}-j+i\}\}$. This happens with probability $\zeta_{j-i+n}^{(K-i)}\binom{\min\{N_{\text{SA}},i\}}{n}\left(\frac{1-\varepsilon}{s}\right)^n\left(1-\frac{1-\varepsilon}{s}\right)^{\min\{N_{\text{SA}},i\}-n}$. Whenever an SA user is scheduled, it leaves SA if the transmitted packet is successfully decoded and there are no more packets. Since the number of packets reported in a BSR is geometrically distributed with mean s, an SA user leaves SA probability $\frac{1-\varepsilon}{s}$ and it stays in SA with probability $1-\frac{1-\varepsilon}{s}$. It is also clear that $j\le\min\{i+N_{\text{RA}},K\}$ because $k_{\text{sa}}\le K$ and no more than N_{RA} UORA users can succeed in a TF cycle. Thus,
$$p_{ij}=\sum_{n=0}^{\min\{N_{\text{SA}},i,K-j,N_{\text{RA}}-j+i\}}\zeta_{j-i+n}^{(K-i)}\binom{\min\{N_{\text{SA}},i\}}{n}\times\frac{(1-\varepsilon)^n(s-1+\varepsilon)^{\min\{N_{\text{SA}},i\}-n}}{s^{\min\{N_{\text{SA}},i\}}},$$
$$\forall 1\le i<K \text{ and } i<j\le\min\{i+N_{\text{RA}},K\}. \quad (27)$$
3) *When $X(t)=i$ and $j<i$: k_{sa}* decreases from i to j if $i-j+n$ SA users depart and n UORA transmissions succeed, where $n\in\{0,1,\dots,\min\{N_{\text{RA}},K-i,j-i+N_{\text{SA}},j\}\}$. This occurs with probability $\left(\frac{1-\varepsilon}{s}\right)^{i-j+n}\times\zeta_n^{(K-i)}\binom{\min\{N_{\text{SA}},i\}}{i-j+n}\left(1-\frac{1-\varepsilon}{s}\right)^{\min\{N_{\text{SA}},i\}-i+j-n}$. It is also clear that $j\ge(i-N_{\text{SA}})^+$ because $k_{\text{sa}}\ge 0$ and no more than N_{SA} SA users leave SA in a TF cycle. Thus,
$$p_{ij}=\sum_{n=0}^{\min\{N_{\text{RA}},K-i,j-i+N_{\text{SA}},j\}}\zeta_n^{(K-i)}\binom{\min\{N_{\text{SA}},i\}}{i-j+n}\times\frac{(1-\varepsilon)^{i-j+n}(s-1+\varepsilon)^{\min\{N_{\text{SA}},i\}-i+j-n}}{s^{\min\{N_{\text{SA}},i\}}},$$
$$\forall 0<i\le K \text{ and } (i-N_{\text{SA}})^+\le j<i. \quad (28)$$
4) *When $X(t)=i=j$:* We have $p_{ii}=1-\sum_{j=0,j\ne i}^{K}p_{ij},\forall 0\le i\le K$.

p_{ij} is 0 for all other i and j. This finite-state DTMC is irreducible and aperiodic. Hence, it has unique steady-state probabilities, which we denote by $\Phi(k)=\Pr(X(t)=k),\forall 0\le k\le K$. In contrast, [4], [5] assume that $k_{\text{sa}}=N_{\text{SA}}$, that is, $\Phi(k)=1$ if $k=N_{\text{SA}}$, and is 0 otherwise. The transition probability diagram of this DTMC is shown in Fig. 2 for $N_{\text{RA}}=2$ and $N_{\text{SA}}=1$.

C. Saturation Throughput Analysis

We now derive expressions for the saturation throughputs of the payload-integrated and time-separated BSR models.

1) Payload-integrated BSR Model: In this model, a TF cycle consists of a TF of duration T_{TF}, a payload frame of duration T_P, and a block ACK frame of duration T_{BACK}, each separated by T_{SIFS} and a propagation delay of duration $\varkappa$. Hence,

$$T_h = T_{\text{TF}} + T_P + T_{\text{BACK}} + 3T_{\text{SIFS}} + 3\varkappa. \tag{29}$$

T_{TF} and T_{BACK} are given as follows. In 802.11ax, a TF consists of a preamble of duration T_{PHY}, a service field of L_{SF} bits, a MAC header of L_{MH} bits, a common information field of 64 bits, a user information field of 48 bits for each SA user, a frame check sequence of L_{FCS} bits, and L_{TB} tail bits [27, subcl. 9.3.1.22.1]. Hence, $T_{\text{TF}} = T_{\text{PHY}} + \left\lceil \frac{L_{\text{SF}}+L_{\text{MH}}+64+48N_{\text{SA}}+L_{\text{FCS}}+L_{\text{TB}}}{\varrho} \right\rceil T_{\text{OFDM}}$, where ϱ is the number of bits per OFDM symbol. Similarly, $T_{\text{BACK}} = T_{\text{PHY}} + \left\lceil \frac{L_{\text{SF}}+L_{\text{MH}}+16+288N_{\text{RU}}+L_{\text{FCS}}+L_{\text{TB}}}{\varrho} \right\rceil T_{\text{OFDM}}$. The TFs and block ACK frames are transmitted with $\varrho = 24$ bits per OFDM symbol.

Let Θ_{UORA} be the UORA saturation throughput and Θ_{SA} be the SA saturation throughput in Mbps.

Result *2:* The UORA saturation throughput is given by

$$\Theta_{\text{UORA}} = \sum_{k_{\text{ra}}=1}^{K} \frac{k_{\text{ra}}\nu_s(k_{\text{ra}}, N_{\text{RA}})T_P\bar{R}}{T_h}\Phi(K - k_{\text{ra}}). \tag{30}$$

Here $\nu_s(k_{\text{ra}}, N_{\text{RA}}) = (1-\varepsilon)\beta(k_{\text{ra}})\left(1 - \frac{\beta(k_{\text{ra}})}{N_{\text{RA}}}\right)^{k_{\text{ra}}-1}$ is the probability of a successful transmission by a tagged UORA user and $\bar{R}$ is the average user throughput with rate adaptation. Since the UORA throughput does not depend on the channel gains of the users, $\bar{R}$ is given by

$$\bar{R} = r_M + \sum_{\tau\in\Delta} \frac{r_\tau - r_{\tau-1}}{\Gamma(m)} \left[\frac{\xi_{m+\frac{1}{\eta}}(m\lambda_\tau D^\eta, m\lambda_\tau L^\eta)}{m^{\frac{1}{\eta}}\lambda_\tau^{\frac{1}{\eta}}(D^2 - L^2)} - \gamma_{\text{inc}}(m, m\lambda_\tau L^\eta) - \frac{D^2}{D^2-L^2}\xi_m(m\lambda_\tau D^\eta, m\lambda_\tau L^\eta) \right], \tag{31}$$

where $\lambda_\tau = \frac{\Upsilon_\tau \sigma^2 (4\pi d_0 f_c)^2}{P_{\text{tx}} d_0^\eta c^2}$, $\xi_p(a,b) = \gamma_{\text{inc}}(p+1, a) - \gamma_{\text{inc}}(p+1, b)$, and $\gamma_{\text{inc}}(.,.)$ is the lower incomplete gamma function [35, Ch. 6].

Proof: Consider an arbitrarily tagged UORA user among the k_{ra} UORA users. This UORA user will successfully transmit a packet in a TF cycle if it transmits on a randomly selected UORA RU, none of the other $(k_{\text{ra}} - 1)$ UORA users transmit on the same RU, and the transmitted packet is decoded successfully, which happen with probabilities $\beta(k_{\text{ra}})$, $\left(1 - \frac{\beta(k_{\text{ra}})}{N_{\text{RA}}}\right)^{k_{\text{ra}}-1}$, and $(1-\varepsilon)$, respectively. Thus the probability $\nu_s(k_{\text{ra}}, N_{\text{RA}})$ of the tagged user successfully transmitting a packet is given by

$$\nu_s(k_{\text{ra}}, N_{\text{RA}}) = (1-\varepsilon)\beta(k_{\text{ra}})\left(1 - \frac{\beta(k_{\text{ra}})}{N_{\text{RA}}}\right)^{k_{\text{ra}}-1}. \tag{32}$$

Each successful UORA user transmits $T_P\bar{R}$ bits in a TF cycle. Hence, the average number of successful UORA transmissions is $k_{\text{ra}}\nu_s(k_{\text{ra}}, N_{\text{RA}})$.[3] Hence, the average number of bits transmitted by k_{ra} users in a TF cycle is equal to $k_{\text{ra}}\nu_s(k_{\text{ra}}, N_{\text{RA}})T_P\bar{R}$. Averaging this over k_{ra} yields (30).

The average user throughput $\bar{R}$ is given by

$$\bar{R} = \sum_{\tau\in\Delta} r_\tau \Pr\left(\Upsilon_\tau \le \frac{P_{\text{tx}} d_0^\eta g_{u,r} c^2}{\sigma^2 d^\eta (4\pi d_0 f_c)^2} < \Upsilon_{\tau+1}\right). \tag{33}$$

Let $\lambda_\tau = \frac{\Upsilon_\tau \sigma^2 (4\pi d_0 f_c)^2}{P_{\text{tx}} d_0^\eta c^2}$. Since $g_{u,r}$ is gamma distributed, we have

$$\Pr\left(\Upsilon_\tau \le \frac{g_{u,r}}{\lambda_\tau} \le \Upsilon_{\tau+1}\right) = \mathbb{E}\left[\Pr\left(g_{u,r} \le \lambda_{\tau+1} d^\eta\right) - \Pr\left(g_{u,r} \le \lambda_\tau d^\eta\right) \middle| d\right], \tag{34}$$

$$= \frac{1}{\Gamma(m)}\mathbb{E}\left[\gamma_{\text{inc}}\left(m, m\lambda_{\tau+1}d^\eta\right) - \gamma_{\text{inc}}\left(m, m\lambda_\tau d^\eta\right)\right], \tag{35}$$

where the last expectation is over the random variable d. Since the users are distributed uniformly within an annular region of inner radius L and outer radius D, the probability density function of d is $2d/(D^2 - L^2)$, for $L \le d \le D$. Let

$$\chi_m \stackrel{\triangle}{=} \mathbb{E}\left[\gamma_{\text{inc}}\left(m, m\lambda_\tau d^\eta\right)\right], \tag{36}$$

$$= \int_L^D \int_0^{m\lambda_\tau d^\eta} \frac{2d}{D^2 - L^2} e^{-t} t^{m-1}\, \mathrm{d}t\, \mathrm{d}d. \tag{37}$$

After several algebraic simplifications, we deduce that

$$\chi_m = \gamma_{\text{inc}}\left(m, m\lambda_\tau L^\eta\right) + \frac{D^2}{D^2 - L^2}\xi_m\left(m\lambda_\tau D^\eta, m\lambda_\tau L^\eta\right) - \frac{1}{D^2 - L^2}\left(m\lambda_\tau\right)^{-\frac{1}{\eta}}\xi_{m+\frac{1}{\eta}}\left(m\lambda_\tau D^\eta, m\lambda_\tau L^\eta\right), \tag{38}$$

where $\xi_p(a,b) = \gamma_{\text{inc}}(p+1, a) - \gamma_{\text{inc}}(p+1, b)$. Substituting (38) and (35) in (33) and simplifying yields (31). ∎

We note that the UORA throughput depends on the number of UORA RUs, the probability of decoding failures, the randomness in the UORA contention process, and the flow of users between UORA and SA.

Result *3:* The SA saturation throughput is given by

$$\Theta_{\text{SA}} = \sum_{k_{\text{sa}}=1}^{K} \frac{\mathbb{E}\left[R(\mathcal{V})|k_{\text{sa}}, N_{\text{SA}}\right] T_P}{T_h}\Phi(k_{\text{sa}}). \tag{39}$$

Here,

$$\mathbb{E}\left[R(\mathcal{V})|k_{\text{sa}}, N_{\text{SA}}\right] = \mathbb{E}\left[\sum_{u\in\mathcal{B}}\sum_{r\in\mathcal{D}} x_{u,r}(\mathcal{V}) R_{u,r} | k_{\text{sa}}, N_{\text{SA}}\right], \tag{40}$$

is the average scheduler throughput with assignment $\mathcal{V}$ in a TF cycle when the number of SA users is k_{sa} and the number of SA RUs is N_{SA}.

Proof: The result follows from the law of total expectation. ∎

We now present expressions for $\mathbb{E}\left[R(\mathcal{V})|k_{\text{sa}}, N_{\text{SA}}\right]$, which appears in (39), for the two schedulers.

[3]This is also equal to $\sum_{n=1}^{\min\{N_{\text{RA}}, k_{\text{ra}}\}} n\zeta_n^{(k_{\text{ra}})}$, where $\zeta_n(k_{\text{ra}})$ is given in (21).

- *Random Scheduler:* Due to the constraints in (3) and (4), the random scheduler can assign at most one user per RU and at most one RU per user. As a result, $\min\{k_{\text{sa}}, N_{\text{SA}}\}$ users are scheduled in a TF cycle and each of them successfully transmits with probability $(1-\varepsilon)$. Hence,

$$\mathbb{E}\left[R(\mathcal{V})|k_{\text{sa}}, N_{\text{SA}}\right] = (1-\varepsilon)\min\{k_{\text{sa}}, N_{\text{SA}}\}\bar{R}. \quad (41)$$

- *Max-throughput Scheduler:* In this scheduler, the assignment of users depends on their channel gains. The assignment variables $x_{u,r}$ are coupled due to the constraints in (3) and (4). As a result, no closed-form expression of $\mathbb{E}\left[R(\mathcal{V})|k_{\text{sa}}, N_{\text{SA}}\right]$ can be derived. Hence, we find $\mathbb{E}\left[R(\mathcal{V})|k_{\text{sa}}, N_{\text{SA}}\right]$ numerically using Monte Carlo simulations by averaging across the channel gains and the distances of the SA users. We tabulate $\mathbb{E}\left[R(\mathcal{V})|k_{\text{sa}}, N_{\text{SA}}\right]$ as a function of $1 \leq k_{\text{sa}} \leq 20$ for $1 \leq N_{\text{SA}} \leq 16$ and $m = 2$ in Appendix C. This needs to be done only once and not in every TF cycle. Also, note that $\mathbb{E}\left[R(\mathcal{V})|k_{\text{sa}}, N_{\text{SA}}\right]$ is not a function of K. Thus, the table does not need to be recomputed for each value of K.

We note that the SA throughput depends on the number of SA RUs, the probability of decoding failures, the average number of packets reported in a BSR, the scheduler assignment, and the flow of users between UORA and SA.

The saturation throughput is equal to $\Theta_{\text{UORA}} + \Theta_{\text{SA}}$.

2) Time-separated BSR Model: In this model, a TF cycle consists of two TFs, each of duration T_{TF}, a BSR frame of duration $T_{\text{BSR}} = \left\lceil \frac{L_{\text{BSR}}}{\varrho} \right\rceil T_{\text{OFDM}}$, a payload frame of duration T_P, and a block ACK frame of duration T_{BACK}, each separated by T_{SIFS} and propagation delay. Hence,

$$T_h = 2T_{\text{TF}} + T_{\text{BSR}} + T_P + T_{\text{BACK}} + 4T_{\text{SIFS}} + 4\varkappa. \quad (42)$$

The expressions for T_{TF} and T_{BACK} are the same for both the models. The expressions for the UORA and SA saturation throughputs in (30) and (39) continue to hold.

D. Average Access Delay Analysis

We now derive the expression for the average access delay ∇ of a user in TF cycles. It is same for the payload-integrated and time-separated BSR models.

Result *4:* The average access delay (in TF cycles) is

$$\nabla = \frac{\sum_{k_{\text{ra}}=1}^{K} k_{\text{ra}}\Phi(K-k_{\text{ra}})}{\sum_{k_{\text{ra}}=1}^{K} k_{\text{ra}}\nu_s(k_{\text{ra}}, N_{\text{RA}})\Phi(K-k_{\text{ra}})}. \quad (43)$$

Proof: The average number of UORA users in a TF cycle is $\sum_{k_{\text{ra}}=1}^{K} k_{\text{ra}}\Phi(K-k_{\text{ra}})$. The average number of UORA users that successfully transmit their BSR packets in a TF cycle is $\sum_{k_{\text{ra}}=1}^{K} k_{\text{ra}}\nu_s(k_{\text{ra}}, N_{\text{RA}})\Phi(K-k_{\text{ra}})$. This is the rate at which the users leave UORA. The expression in (43) then follows from Little's theorem [34, Ch. 5.5]. ■

We note that the average access delay depends on the number of UORA RUs, the randomness in the UORA contention process, and the flow of users between UORA and SA.

IV. Optimal RU Allocation Policy Design

In this section, we determine an optimal RU allocation policy. We use the Markovian evolution of the system and the analytical results derived in Section III to model the RU allocation problem as an MDP in Section IV-A. Then, we use relative value iteration to determine an optimal RU allocation policy in Section IV-B. In Section IV-C, we analyze the saturation throughput and the average access delay of the optimal policy. Lastly, in Section IV-D, we design an optimal RU allocation policy when the number of packets reported in the BSR follows a general distribution.

A. MDP Specification

An MDP is represented by the tuple $\mathcal{Q} = (\mathcal{S}, \mathcal{A}, P, W)$, where $\mathcal{S}$ is the state space, $\mathcal{A}$ is the action space, P is the transition probability function, and W is the reward function. The elements of $\mathcal{Q}$ are specified as follows:

1) *State Space:* The state is the number of SA users k_{sa} at the beginning of a TF cycle. Hence, $\mathcal{S} = \{0, 1, \ldots, K\}$.
2) *Action Space:* The action is the number of UORA RUs N_{RA} allocated at the beginning of a TF cycle. Hence, $\mathcal{A} = \{0, 1, \ldots, N_{\text{RU}}\}$.
3) *Transition Function:* The transition function is a mapping $P : \mathcal{S} \times \mathcal{S} \times \mathcal{A} \to [0, 1]$. We denote the entries of P as $P(j|i, a) = \Pr(X(t+1) = j | X(t) = i, a_t = a)$. It represents the transition probability from state i to state j when the state at time t is i and action $a_t = a$ is taken. We have derived these transition probabilities in Section III-B. Note that they are not a function of t.
4) *Reward Function:* The reward function is a mapping $W : \mathcal{S} \times \mathcal{A} \to \mathbb{R}$. Here, $W(i, a)$ is the reward obtained when action a is taken in state i. We consider the following reward function:

$$W(i, a) = Y(i, a) + Z(i, a) - qD(i, a). \quad (44)$$

Here $Y(i, a)$ is the UORA throughput, $Z(i, a)$ is the SA throughput, and $D(i, a)$ is the access delay when the number of SA users is i and the number of UORA RUs is a. A larger $q \geq 0$ gives more importance to the access delay. The reward function increases as the saturation throughput increases and decreases as the access delay increases. It captures the aforementioned trade-off between the saturation throughput and the access delay. The UORA throughput also needs to be considered in the total throughput because a UORA user transmits data along with its BSR. Here, $Y(i, a)$, $Z(i, a)$, and $D(i, a)$ are random since they depend on the randomness of the UORA transmissions and the scheduler assignments in SA.

Algorithm 1: ODRAP design using RVI approach

Input: $\mathcal{S}, \mathcal{A}, P, W, \theta > 0$
Initialize: Set $n = 0, v_n(i) = 0, u_n(i) = 0,\ \forall i \in \mathcal{S}$, and choose $\hat{i} \in \mathcal{S}$
Repeat:
for $i \in \mathcal{S}$ **do**
  for $a \in \mathcal{A}$ **do**
    Compute the value function for each i and a;
    $g(i,a) = w(i,a) + \sum_{j \in \mathcal{S}} P(j|i,a)\, u_n(j)$;
  end
  Find the optimal value function for each i:
  $v_{n+1}(i) = \max_{a \in \mathcal{A}} \{g(i,a)\}$;
end
Subtract $v_{n+1}(\hat{i})$ from the optimal value function:
$u_{n+1}(i) = v_{n+1}(i) - v_{n+1}(\hat{i}),\ \forall i \in \mathcal{S}$;
$n = n + 1$;
Until: $|v_{n+1}(i) - v_n(i)| < \theta,\ \forall i \in \mathcal{S}$;
For each $i \in \mathcal{S}$, choose the optimal action
$\pi^\star(i) = \arg\max_{a \in \mathcal{A}} \left\{ w(i,a) + \sum_{j \in \mathcal{S}} P(j \mid i,a) v_n(j) \right\}$;
Output: π^*

B. Optimal Dynamic RU Allocation Policy

We employ an infinite-horizon MDP model to derive a dynamic RU allocation policy (ODRAP) that optimizes the long-term reward. Since $\mathcal{S}$ and $\mathcal{A}$ are finite, W is bounded above, and the underlying DTMC is irreducible and aperiodic under all the stationary policies, a stationary optimal policy exists [36, Ch. 3]. The system's stationary characteristics justify the use of an infinite-horizon MDP [36, Ch. 1]. We consider the average reward criterion in our MDP setup. On the other hand, the discounted reward MDP is better suited for scenarios where future rewards have diminishing importance.

Let Π denote the set of all dynamic RU allocation policies. We employ the relative value iteration (RVI) approach to find ODRAP $\pi^* \in \Pi$. Let $v_n(i)$ and $u_n(i)$, $\forall i \in \mathcal{S}$, denote the value and relative value functions, respectively, in iteration n. At $n = 0$, we initialize $v_n(i)$ and $u_n(i)$ to 0, $\forall i \in \mathcal{S}$, and choose an arbitrary state $\hat{i} \in \mathcal{S}$. For $n \geq 0$, we determine the optimal value function $v_{n+1}(i)$, $\forall i \in \mathcal{S}$, by maximizing the expression [37, Ch. 8.5.5]

$$g(i,a) = w(i,a) + \sum_{j \in \mathcal{S}} P(j|i,a)\, u_n(j),\ \forall a \in \mathcal{A}, \tag{45}$$

where $w(i,a) = \mathbb{E}[W(i,a)]$. We find the optimal action $\pi^*(i)$ that achieves this optimal value for each state i.

A key point to note is that the algorithm requires only the average value of the reward, $w(i,a)$. We derive an expression for it below. Here, $w(i,a) = y(i,a) + z(i,a) - qd(i,a)$, where $y(i,a) = \mathbb{E}[Y(i,a)]$, $z(i,a) = \mathbb{E}[Z(i,a)]$, and $d(i,a) = \mathbb{E}[D(i,a)]$.

After determining $v_n(i)$, $\forall i \in \mathcal{S}$, we update the relative value function $u_n(i)$ by subtracting $v_n(\hat{i})$ from $v_n(i)$, $\forall i \in \mathcal{S}$. Here, $\hat{i} \in \mathcal{S}$ is used to normalize the value function to prevent it from diverging. Such re-normalizing in every iteration avoids a divergence of the value function [37, Ch. 8.5.5]. We use the updated relative value function $u_n(i)$ to compute $g(i,a)$ and find $\pi^*(i)$ in the next step for each i. We repeat this process until the change in $v_n(i),\ \forall i \in \mathcal{S}$, becomes sufficiently small. We note that ODRAP needs to be designed only once. The pseudo-code to find ODRAP is given in Algorithm 1.

Expression for $w(i,a)$: From Results 2 and 3, we have

$$y(i,a) = \begin{cases} \frac{(K-i)\nu_s(K-i,a)T_P\bar{R}}{T_h}, & \forall i > 0, a > 0, \\ 0, & \text{otherwise}, \end{cases} \tag{46}$$

$$z(i,a) = \frac{\mathbb{E}[R(\mathcal{V})|i, N_{\text{RU}} - a]\, T_P}{T_h},\ \forall i, a. \tag{47}$$

The expression for $d(i,a)$ is given below.

Lemma *3:* The average access delay $d(i,a)$ (in TF cycles) when $k_{\text{ra}} = K - i$ and $N_{\text{RA}} = a$ is given by

$$d(i,a) = \begin{cases} \frac{1}{\nu_s(K-i,a)}, & \forall i < K, a > 0, \\ \infty, & \forall i < K, a = 0, \\ 0, & \text{otherwise}. \end{cases} \tag{48}$$

Proof: From the decoupling approximations, the instant at which a successful transmission, collision, or idle period ends is a renewal instant. With probability $\nu_s(K-i,a)$, a successful transmission occurs and the access delay is 1. With probability $\nu_c(K-i,a)$, a collision occurs and the average access delay is $1 + d(i,a)$. Similarly, with probability $1 - \nu_s(K-i,a) - \nu_c(K-i,a)$, an idle period occurs and the average access delay is $1 + d(i,a)$. Hence,

$$\begin{aligned} d(i,a) &= \nu_s(K-i,a) + \nu_c(K-i,a)(1 + d(i,a)) \\ &\quad + (1 - \nu_s(K-i,a) - \nu_c(K-i,a))(1 + d(i,a)). \end{aligned} \tag{49}$$

Rearranging the terms yields the first case in (48). The other two cases are straightforward. ■

Note that the above expressions are the outcome of the analytical framework presented in Section III.

Remark: Fixing $a = N_{\text{RA}}$ and taking the average of $d(i,a)$ in (48) with respect to the steady-state distribution of the DTMC $X(t),\ t \geq 1$, which is described in Section III-B, also gives (43).

C. Analysis of ODRAP

We now generalize the saturation throughput and average access delay analysis in Section III, which was for a static RU allocation, for ODRAP, which is a dynamic RU allocation policy. For this, we construct a new DTMC where the number of UORA RUs, N_{RA} and the number of SA RUs, N_{SA} are obtained from the optimal policy $\pi^*(.)$. Thus, $N_{\text{RA}} = \pi^*(k_{\text{sa}})$ and $N_{\text{SA}} = N_{\text{RU}} - \pi^*(k_{\text{sa}})$. Therefore, substituting $N_{\text{RA}} = \pi^*(k_{\text{sa}})$, where $k_{\text{sa}} = K - k_{\text{ra}}$, in (6) and (13) gives the expressions for the conditional collision probability $\alpha(k_{\text{ra}})$ and the attempt rate $\beta(k_{\text{ra}})$. Similarly, substituting $N_{\text{RA}} = \pi^*(k_{\text{sa}})$ in (21) and the DTMC transition probabilities in Section III-B gives the expressions for $\zeta_n^{(k_{\text{ra}})}$ and p_{ij}. The steady-state probabilities for ODRAP are unique because the

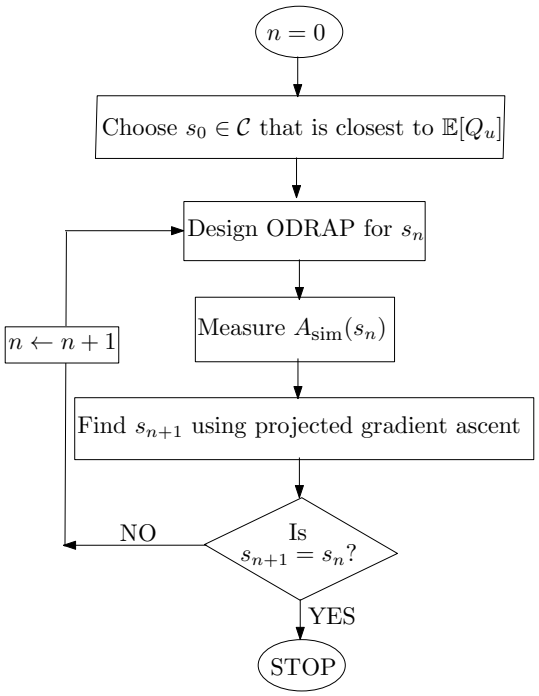

Fig. 3. Iterative approach to design ODRAP for a general buffer distribution.

TABLE III
802.11AX-SPECIFIC SIMULATION PARAMETERS

Parameter	Value	Parameter	Value	Parameter	Value
L_{SF}	16 bits	$\varkappa$	3 μs	Bandwidth	160 MHz
L_{FCS}	32 bits	T_P	5 ms	f_c	5 GHz
L_{MH}	128 bits	T_{PHY}	20 μs	N_{RU}	16
L_{TB}	6 bits	T_{SIFS}	16 μs	$C_{\min}$	16
L_{BSR}	256 bits	T_{OFDM}	4 μs	$C_{\max}$	1024

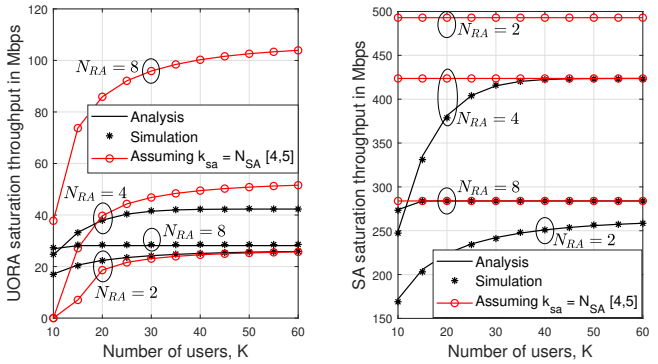

(a) UORA (b) SA

Fig. 4. UORA and SA saturation throughputs as a function of K for different values of N_{RA} ($s = 10$). Note that the y-axis ranges in the two sub-figures are different.

underlying DTMC is finite, irreducible, and aperiodic under all the stationary policies.

The expressions for the UORA and SA saturation throughputs and the average access delay are the same as those in Results 2, 3, and 4 except that the probability of successful transmission of a tagged UORA user changes to

$$\nu_s(k_{\text{ra}}, \pi^*(k_{\text{sa}})) = \beta(k_{\text{ra}}) \left(1 - \frac{\beta(k_{\text{ra}})}{\pi^*(k_{\text{sa}})}\right)^{k_{\text{ra}}-1}, \qquad (50)$$

and the average scheduler throughput $\mathbb{E}\left[R(\mathcal{V})|k_{\text{sa}}, N_{\text{SA}}\right]$ is evaluated for $N_{\text{SA}} = N_{\text{RU}} - \pi^*(k_{\text{sa}})$.

D. Extending ODRAP to Arbitrary Buffer Distributions

We now extend our analytical framework to arbitrary buffer distributions. Let an SA user u report $Q_u \in \{1, 2, \ldots, D\}$ packets in its BSR to the AP, where D is the maximum number of packets that can be reported. Unlike Section III-B, Q_u need not be a geometric RV.

Let $X_j(t)$ represent the number of SA users in TF cycle t that have j packets remaining to be sent. Hence, $\sum_{j=1}^{D} X_j(t) = k_{\text{sa}}$. The state of the system in TF cycle t now becomes $\mathbf{X}(t) = (X_1(t), X_2(t), \ldots, X_D(t))$. This follows from the decoupling approximations, which imply that $\mathbf{X}(t), t \geq 1$, is a DTMC. It has $O(K^D)$ states. However, the large number of states makes an exact analysis intractable, and the MDP-based policy design becomes challenging.

We present an iterative approach to address this challenge. It consists of two stages. The first is a pre-compute stage. In it, we design ODRAP for each s in $\mathcal{C} = \{s_{\min} + n\delta : n = 0, 1, 2, \ldots, \frac{s_{\max} - s_{\min}}{\delta}\}$, where δ is the granularity. Therefore, $\mathcal{C}$ consists of $\frac{s_{\max} - s_{\min}}{\delta} + 1$ elements. These policies can be precomputed and stored in a lookup table.

In the second stage, we utilize the projected gradient ascent algorithm [38, Ch. 8] to determine the optimal value of s that achieves the largest reward among the class of policies designed for geometric buffer distributions. Let $A_{\text{sim}}(s)$ denote the average reward measured from Monte Carlo simulations for the given general buffer distribution while using the RU allocation designed by ODRAP, as per Section IV-B, for a geometric buffer distribution with mean s.

We set the initial value $s_0 \in \mathcal{C}$ as the one that is closest to $\mathbb{E}[Q_u]$. We measure $A_{\text{sim}}(s_0 + \delta)$ and $A_{\text{sim}}(s_0 - \delta)$. We compute the gradient $\nabla A_{\text{sim}}(s_0) = \frac{A_{\text{sim}}(s_0+\delta) - A_{\text{sim}}(s_0-\delta)}{2\delta}$ and find $s_1 \in \mathcal{C}$ using the projected gradient ascent algorithm. Then, we measure $A_{\text{sim}}(s_1 + \delta)$ and $A_{\text{sim}}(s_1 - \delta)$, and as above, find s_2. We repeat this process until we find the value of s that maximizes $A_{\text{sim}}(s)$. Fig. 3 illustrates this approach.

Given the involved dynamics, no proof of convergence is possible. However, we have found that this approach converges in practice within 7 iterations.

V. RESULTS AND DISCUSSIONS

We now present Monte Carlo simulation results to quantify the impact of the system parameters and to assess the efficacy of our design. We implement the 802.11ax PHY and MAC layers in Matlab as simulators such as ns-3 and Opnet do not yet have all the necessary modules to support hybrid access OFDMA. The simulations are run over 10^6 TF cycles. Table III lists the 802.11ax-specific simulation parameters. The path-

This article has been accepted for publication in IEEE Transactions on Mobile Computing. This is the author's version which has not been fully edited and content may change prior to final publication. Citation information: DOI 10.1109/TMC.2025.3634127

loss parameters are: $c = 3 \times 10^8$ m/s, $\eta = 3.8$, $d_0 = 1$ m, $d_{\max} = 50$ m, $P_{\text{tx}} = 30$ dBm, $\sigma^2 = -105$ dBm, and $m = 2$.

We first present results for the static RU allocation policies and then for the dynamic policies. Unless mentioned otherwise, the results are for the payload-integrated BSR model and the random scheduler.

A. Static RU Allocation

1) Saturation Throughput: Fig. 4a shows the UORA saturation throughput as a function of the number of users K for different values of N_{RA}. As K increases, the UORA throughput increases because the number of successful UORA transmissions increases; it eventually saturates due to increased contention in UORA. As N_{RA} increases, the UORA throughput first increases because the users can contend over more RUs, which increases the odds of success in each UORA RU. However, when N_{RA} increases from 4 to 8, the UORA throughput decreases. This is because when N_{RA} is large, fewer users remain in UORA and contribute to the UORA throughput. The analysis and simulation results are within 3% of each other for all the values of N_{RA} and K. We also plot the UORA throughput when k_{sa} is assumed to be fixed, as done in [4], [5]. We observe that this assumption underestimates the UORA throughput when $N_{\text{RA}} = 2$, but overestimates the UORA throughput when $N_{\text{RA}} = 4$ and 8.

Fig. 4b shows the corresponding SA saturation throughput. As K increases, the average number of SA users increases because the number of successful UORA transmissions increases. Consequently, the AP schedules more SA users, and the SA throughput increases. The SA throughput also increases when N_{RA} increases from 2 to 4 because more users can successfully contend in UORA and enter SA. However, it decreases when N_{RA} increases from 4 to 8 because fewer RUs are available for SA. The analysis and simulation throughput results are within 2% of each other for all the values of N_{RA} and K. We also plot the SA throughput when k_{sa} is assumed to be fixed, as done in [4], [5]. We observe that this assumption overestimates the SA throughput since it assumes all the SA RUs are always occupied. This effect is most perceptible for $N_{\text{RA}} = 2$. The SA throughput is greater than the UORA throughput due to the contention-free transmissions in SA.

Fig. 5 compares the saturation throughputs of the payload-integrated and time-separated BSR models. The throughputs of both models increase as K increases since both UORA and SA throughputs increase. As N_{RA} increases, the throughputs first increase and then decrease. This follows the trends for the SA throughput, which is more than the UORA throughput. The throughput of the payload-integrated model is 5.7% to 7.2% more than that of the time-separated model, which incurs an additional time overhead as the UORA and SA transmissions occur separately in different TF cycles. The analysis and simulation results are within 2% of each other for both models. This again validates our approach of assuming a steady state and then averaging over different values of k_{sa} as per the DTMC model. Our results remain accurate even for

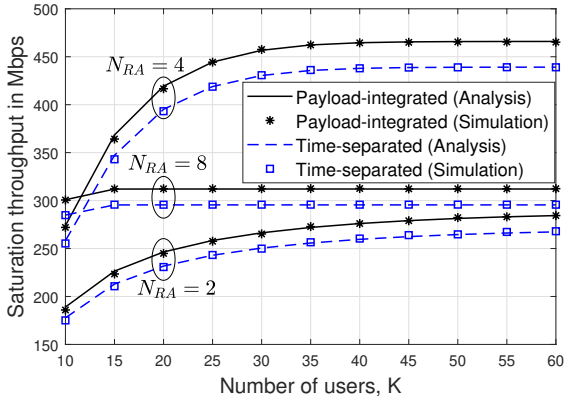

Fig. 5. Saturation throughput of the payload-integrated and time-separated BSR models as a function of K for different values of N_{RA} ($s = 10$).

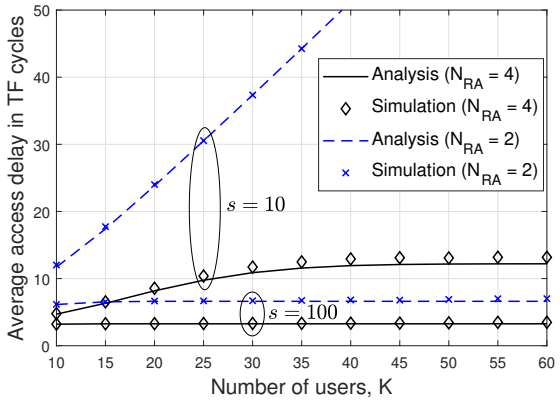

Fig. 6. Average access delay as a function of K for different values of N_{RA} and s.

K as large as 100. We present them up to $K = 60$ because the throughput does not change for larger K.

2) Average Access Delay: Fig. 6 plots the average access delay as a function of K for different values of N_{RA} and s. The access delay first increases as K increases because of increased contention in UORA, which increases the time a user waits to successfully transmit its BSR packet. For $N_{\text{RA}} = 4$, the access delay saturates for larger K because more users successfully transmit their BSRs and transition from UORA to SA. Consequently, users spend longer durations in SA awaiting their scheduled transmissions. The average number of SA users increases, while the average number of UORA users saturates as K increases. Thus, the access delay also saturates. However, for $N_{\text{RA}} = 2$ and $s = 10$, the average access delay increases as K increases and does not saturate. This is because the large number of SA RUs and smaller s implies that users spend less time in SA and come back to UORA after transmitting their packets. The access delay decreases as N_{RA} increases because the number of successful UORA transmissions increases. The access delay decreases as s increases for both $N_{\text{RA}} = 2$ and 4. This is because each

This article has been accepted for publication in IEEE Transactions on Mobile Computing. This is the author's version which has not been fully edited and content may change prior to final publication. Citation information: DOI 10.1109/TMC.2025.3634127

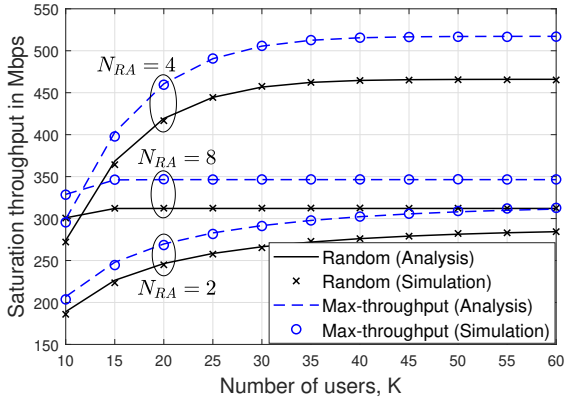

Fig. 7. Effect of scheduler: Saturation throughput of random and max-throughput schedulers as a function of K for different values of N_{RA} ($s = 10$).

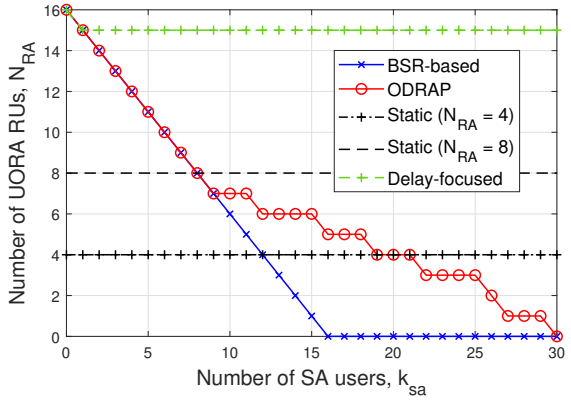

Fig. 8. Number of UORA RUs as a function of k_{sa} for different RU allocation policies ($s = 10$ and $K = 30$).

user stays in SA for more TF cycles. This reduces the average number of UORA users and increases the probability of a successful UORA transmission.

The analysis and simulation results differ by less than 8% for $N_{\text{RA}} = 4$. The gap is less than 2% for $N_{\text{RA}} = 2$. Compared to $N_{\text{RA}} = 2$, the number of UORA users who move to SA is larger, on average, for $N_{\text{RA}} = 4$. Similarly, the number of users who move from SA to UORA is also larger. Since the accuracy of the analysis depends on how quickly the system settles into a steady state, the results for $N_{\text{RA}} = 2$ are marginally more accurate than for $N_{\text{RA}} = 4$.

3) Impact of Scheduler: Fig. 7 compares the saturation throughputs of the random and max-throughput schedulers. It plots the throughput as a function of K. The analysis and simulation results are within 2% of each other for both schedulers for all values of K. As before, the throughput increases as K increases for both schedulers for any N_{RA}. The max-throughput scheduler has a greater throughput than the random scheduler, which does not exploit multi-user diversity and instead focuses on ensuring fairness. The results bring out the dependence of the max-throughput scheduler's throughput on the number of RUs allocated for UORA. When $N_{\text{RA}} = 4$, the max-throughput scheduler has 9.2% to 11.1% greater throughput than the random scheduler as K increases from 10 to 100. When $N_{\text{RA}} = 8$, the corresponding increase is 10.9% to 11.2%. For $N_{\text{RA}} = 2$, the corresponding gains are marginally lower and are 9.3% to 9.6%.

B. Dynamic RU Allocation

We now benchmark ODRAP with the dynamic policies, namely, BSR-based [4], [5] and delay-focused RU allocation. The delay-focused RU allocation policy reduces the average access delay by assigning all the RUs to UORA if no SA users are present and by reserving the bare minimum of one RU for SA when at least one SA user exists. Furthermore, we benchmark ODRAP with the static policies [4], [5], [22], [23], with $N_{\text{RA}} = 4$ and 8 and $q = 3$. We compare the average

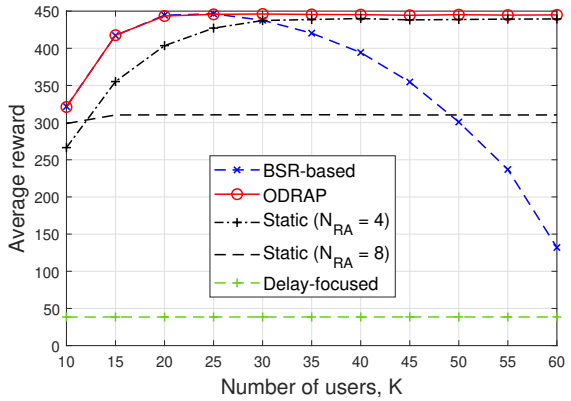

Fig. 9. Average reward as a function of K for different RU allocation policies ($s = 10$).

reward and study how the different policies trade-off saturation throughput and average access delay.

1) Geometric Buffer Distribution: Fig. 8 shows N_{RA} as a function of k_{sa} for the BSR-based, ODRAP, delay-focused, and static policies for $s = 10$ and $K = 30$. In the static RU allocation policy, N_{RA} is a horizontal line as it is fixed. The delay-focused policy assigns the most number of RUs to UORA to minimize the access delay. However, the ODRAP and BSR-based RU allocation policies assign fewer RUs for UORA as k_{sa} increases. For smaller k_{sa}, ODRAP and the BSR-based policy assign the same number of RUs for UORA. This is because the saturation throughput-related term dominates the reward in (44) as the access delay is small. However, these two policies differ for larger k_{sa}. The BSR-based policy allocates no RUs to UORA for $k_{\text{sa}} \geq N_{\text{RU}}$, which increases the access delay. On the other hand, the decrease in N_{RA} is more gradual for ODRAP as the access delay depends on N_{RA}, as we saw in Fig. 6.

Fig. 9 plots the average reward as a function of K for all the policies. ODRAP has the largest average reward among all the policies for all K, which shows the effectiveness of our MDP-

This article has been accepted for publication in IEEE Transactions on Mobile Computing. This is the author's version which has not been fully edited and content may change prior to final publication. Citation information: DOI 10.1109/TMC.2025.3634127

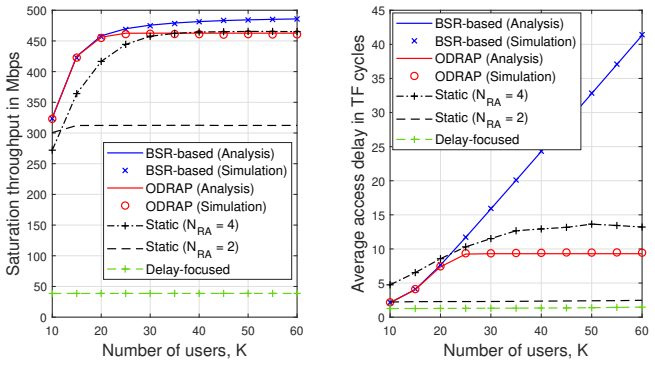

(a) Saturation throughput (b) Average access delay

Fig. 10. Saturation throughput and average access delay as a function of K for different RU allocation policies ($s = 10$).

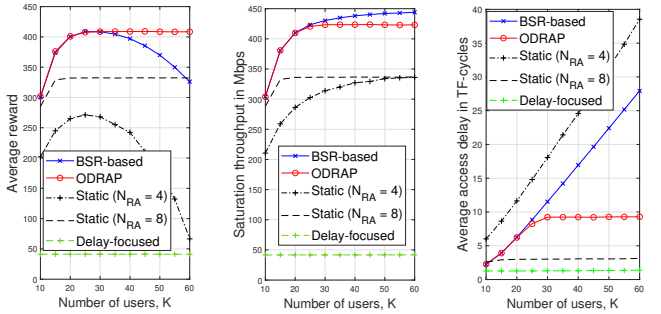

(a) Average reward (b) Saturation throughput (c) Average access delay

Fig. 11. Average reward, saturation throughput, and average access delay as a function of K for different RU allocation policies for a uniform buffer distribution.

based design. As K increases, the average rewards of ODRAP and the static policies first increase and then saturate. On the other hand, the reward of the BSR-based policy initially increases but collapses for larger K. The delay-focused policy has the lowest reward. The static policy with $N_{\text{RA}} = 4$ is close to ODRAP for $K \geq 30$. However, this is not true for all values of s. For example, we shall see in Fig. 11a, when the average number of packets reported in a BSR is 5.5, the static policy with $N_{\text{RA}} = 4$ is far from optimal. To understand the above trends, we separately study the saturation throughputs and average access delays of all the policies in Fig. 10.

Fig. 10a compares the saturation throughputs as a function of K for all the policies for the random scheduler. Similar to Fig. 5, the saturation throughputs of all the policies increase as K increases and saturate for larger K. The BSR-based RU allocation policy has a marginally higher throughput than ODRAP, especially at larger K, since it maximizes the contention-free SA throughput by allocating as many RUs as possible to serve all the SA users. The delay-focused policy has the lowest throughput. The throughputs of the static policies depend on N_{RA}.

Fig. 10b plots the corresponding results for the average access delay. The access delays of all the policies increase as K increases due to the increased contention in UORA. The BSR-based policy and ODRAP have the same access delay for small K. However, as K increases, the access delay of the BSR-based policy increases much more than that of ODRAP, which sets aside more RUs for UORA. The delay-focused policy has the lowest access delay since it always allocates more RUs for UORA. The access delays of the static policies can be either more or less than that of ODRAP, depending on the choice of N_{RA}. The simulation and analysis results for ODRAP and the BSR-based policy in Figs. 10a and 10b are within 4% of each other. This verifies the applicability of our analysis to dynamic RU allocation policies.

Appendix D studies the saturation throughput and the access delay of ODRAP for the random and the max-throughput schedulers. The trends are qualitatively similar to those in Fig. 7, with the max-throughput scheduler achieving a higher throughput. The average access delay does not depend on the scheduler because it does not impact the flow of users between UORA and SA.

2) Non-geometric Buffer Distribution: Fig. 11a plots the average reward as a function of K for the BSR-based, ODRAP, delay-focused, and static policies when the number of packets reported in the BSR is uniformly drawn from the set $\{1, 2, \ldots, 10\}$. We design ODRAP for this distribution using the iterative approach in Section IV-D with $s_{\min} = 4$, $s_{\max} = 7$, and $\delta = 0.1$. The optimal value of s for which the average reward $A_{\text{sim}}(s)$ is maximized turns out to be 5.5 for all K. ODRAP has the largest reward for all K among all the policies, which shows its effectiveness. The average rewards of ODRAP and the static policy with $N_{\text{RA}} = 8$ first increase as K increases and saturate for larger K. On the other hand, the average rewards of the BSR-based policy and the static policy with $N_{\text{RA}} = 4$ decrease for larger K due to their larger access delays. As before, the delay-focused policy has the lowest average reward. Figs. 11b and 11c separately plot the saturation throughputs and the average access delays for all the policies. The trends are similar to those in Fig. 10.

VI. Conclusions

We analyzed the saturation throughput and the average access delay of hybrid access in an 802.11ax uplink for static as well as dynamic RU allocation policies. The analysis accounted for contention-based UORA and contention-free SA, and the dynamic flow of users between them. It also modeled discrete rate adaptation, packet decoding errors, and the impact of the AP's scheduler. The renewal-theoretic, fixed-point analysis and Markov model of the number of UORA and SA users led to an accurate characterization of the saturation throughput and the average access delay. The analysis enabled the design of a dynamic RU allocation policy that optimized a long-term reward using the relative value iteration approach. We first designed the dynamic policy for the geometric buffer distribution and then extended it to general buffer distribu-

tions. This is unlike the literature that has focused on ad hoc designs.

The optimal policy adapted the RU allocation as a function of the number of SA users to balance between the saturation throughput and the average access delay. It differed from the conventional BSR-based policy that assigned fewer RUs for UORA and static policies. The saturation throughput and the average access delay of the max-throughput scheduler depended on the number of RUs allocated to UORA.

Interesting avenues for future work include analyzing the statistics of packet delays for hybrid access with unsaturated traffic, and modeling legacy users and multiple APs and the interactions between them.

REFERENCES

[1] S. Arthi and N. B. Mehta, "Saturation throughput analysis of hybrid access MAC protocol in IEEE 802.11ax WLANs," in *Proc. GLOBECOM*, Dec. 2024, pp. 1–6.

[2] E. Khorov, A. Kiryanov, A. Lyakhov, and G. Bianchi, "A tutorial on IEEE 802.11ax high efficiency WLANs," *IEEE Commun. Surveys Tuts.*, vol. 21, no. 1, pp. 197–216, 1st Qtr. 2019.

[3] B. Bellalta and K. Kosek-Szott, "AP-initiated multi-user transmissions in IEEE 802.11ax WLANs," *Ad Hoc Netw.*, vol. 85, pp. 145–159, Mar. 2019.

[4] S. Bhattarai, G. Naik, and J.-M. J. Park, "Uplink resource allocation in IEEE 802.11ax," in *Proc. ICC*, May. 2019, pp. 1–6.

[5] A. Behara and T. G. Venkatesh, "Performance analysis and energy efficiency of MU-(OFDMA & MIMO) based hybrid MAC protocol of IEEE 802.11ax WLANs," *IEEE Trans. Veh. Technol.*, vol. 72, no. 5, pp. 6474–6490, May 2023.

[6] L. Lanante, H. O. T. Uwai, Y. Nagao, M. Kurosaki, and C. Ghosh, "Performance analysis of the 802.11ax UL OFDMA random access protocol in dense networks," in *Proc. ICC*, May 2017, pp. 1–6.

[7] R.-G. Cheng, C.-M. Yang, B. S. Firmansyah, and R. Harwahyu, "Uplink OFDMA-based random access mechanism with bursty arrivals for IEEE 802.11ax systems," *IEEE Netw. Lett.*, vol. 4, no. 1, pp. 34–38, Mar. 2022.

[8] J. Yang, R. He, X. Fang, L. Yan, and H. Ju, "Random access modelling and performance analysis for the 802.11ax UORA mechanism in multiple BSSs," in *Proc. VTC Fall*, Sep. 2022, pp. 1–6.

[9] A. Rehman, F. B. Hussain, R. Ali, and T. Khurshaid, "Collision-based up-link OFDMA random access mechanism for Wi-Fi 6," *IEEE Access*, vol. 11, pp. 117 094–117 109, 2023.

[10] H.-W. Tseng, T.-T. Yang, and B.-H. Tsai, "Priority-based resource reservation mechanism for uplink multi-user transmission in IEEE 802.11ax networks," in *Proc. ICC*, May 2023, pp. 2535–2540.

[11] K. Kosek-Szott, S. Szott, and F. Dressler, "Improving IEEE 802.11ax UORA performance: Comparison of reinforcement learning and heuristic approaches," *IEEE Access*, vol. 10, pp. 120 285–120 295, 2022.

[12] N. Cordeschi, W. Zhuang, R. Tafazolli, and Y. Gao, "Optimal random access strategies for trigger-based multiple-packet reception channels," *IEEE Trans. Mob. Comput.*, vol. 23, no. 3, pp. 2303–2320, Mar. 2024.

[13] M. Han, X. Sun, W. Zhan, Y. Gao, and Y. Jiang, "Multi-agent reinforcement learning based uplink OFDMA for IEEE 802.11ax networks," *IEEE Trans. on Wireless Commun.*, vol. 23, no. 8, pp. 8868–8882, Aug. 2024.

[14] M. Jin, J. Meng, W. Wu, and Y. Liu, "Enhancing the performance of Wi-Fi 7 network via investigation of multi-link and UORA," *IEEE Commun. Lett.*, vol. 28, no. 11, pp. 2688–2692, Nov. 2024.

[15] D. Magrin, S. Avallone, S. Roy, and M. Zorzi, "Performance evaluation of 802.11ax OFDMA through theoretical analysis and simulations," *IEEE Trans. Wireless Commun.*, vol. 22, no. 8, pp. 5070–5083, Aug. 2023.

[16] Y. Kim, G. Kim, Y. Oh, and W. Choi, "Transmission delay-based uplink multi-user scheduling in IEEE 802.11ax networks," *Appl. Sci.*, vol. 11, pp. 1–19, Oct. 2021.

[17] D. Bankov, A. Didenko, E. Khorov, and A. Lyakhov, "OFDMA uplink scheduling in IEEE 802.11ax networks," in *Proc. ICC*, May 2018, pp. 1–6.

[18] K.-H. Lee, "Using OFDMA for MU-MIMO user selection in 802.11ax-based Wi-Fi networks," *IEEE Access*, vol. 7, pp. 186 041–186 055, Dec. 2019.

[19] K. Wang and K. Psounis, "Efficient scheduling and resource allocation in 802.11ax multi-user transmissions," *Comput. Commun.*, vol. 152, pp. 171–186, Feb. 2020.

[20] K. Dovelos and B. Bellalta, "A scheduling policy for downlink OFDMA in IEEE 802.11ax with throughput constraints," *arXiv:2009.00413*, Sep. 2020. [Online]. Available: https://arxiv.org/pdf/2009.00413.pdf

[21] H. Noh, H. Lee, and H. J. Yang, "Joint optimization on uplink OFDMA and MU-MIMO for IEEE 802.11ax: Deep hierarchical reinforcement learning approach," *To appear in IEEE Commun. Lett.*, 2024.

[22] M. Peng, Q. Yin, K. Zhang, and C. Kai, "Adaptive multi-user uplink resource allocation based on access delay analysis in IEEE 802.11ax," *Wirel. Netw.*, vol. 29, p. 1223–1235, Nov. 2022.

[23] K.-H. Lee, "Performance analysis of the IEEE 802.11ax MAC protocol for heterogeneous Wi-Fi networks in non-saturated conditions," *Sens.*, vol. 19, pp. 1–20, Mar. 2019.

[24] A. Kumar, E. Altman, D. Miorandi, and M. Goyal, "New insights from a fixed-point analysis of single cell IEEE 802.11 WLANs," *IEEE/ACM Trans. Netw.*, vol. 15, no. 3, pp. 588–601, Jun. 2007.

[25] G. Bianchi, "Performance analysis of the IEEE 802.11 distributed coordination function," *IEEE J. Sel. Areas Commun.*, vol. 18, no. 3, pp. 535–547, Mar. 2000.

[26] G. Naik, S. Bhattarai, and J.-M. Park, "Performance analysis of uplink multi-user OFDMA in IEEE 802.11ax," in *Proc. ICC*, May. 2018, pp. 1–6.

[27] "IEEE standard for information technology–telecommunications and information exchange between systems local and metropolitan area networks–specific requirements part 11: Wireless LAN medium access control (MAC) and physical layer (PHY) specifications amendment 1: Enhancements for high-efficiency WLAN," *IEEE Std 802.11ax-2021 (Amendment to IEEE Std 802.11-2020)*, pp. 1–767, May 2021.

[28] A. Goldsmith, *Wireless Communications*, 1st ed. Cambridge Univ. Press, 2005.

[29] H. Hashemi, "The indoor radio propagation channel," *Proc. IEEE*, vol. 81, no. 7, pp. 943–968, Jul. 1993.

[30] nsnam.org.2020, "ns3 Wi-Fi module." [Online]. Available: https://www.nsnam.org/docs/models/html/wifi-design.html#tablebasederrorratemodel

[31] D. B. West, *Introduction to Graph Theory*, 2nd ed. Prentice Hall, 2000.

[32] G. Sharma, A. Ganesh, and P. Key, "Performance analysis of contention based medium access control protocols," *IEEE Trans. Inf. Theory*, vol. 55, no. 4, pp. 1665–1682, Apr. 2009.

[33] C. Bordenave, D. Mcdonald, and A. Proutière, "Random multi-access algorithms - a mean field analysis," INRIA, Research report RR-5632, 2005. [Online]. Available: https://inria.hal.science/inria-00070375

[34] R. G. Gallager, *Stochastic Processes: Theory for Applications*, 1st ed. Cambridge Univ. Press, 2013.

[35] M. Abramowitz and I. A. Stegun, *Handbook of Mathematical Functions with Formulas, Graphs, and Mathematical Tables,*, 9th ed. Dover Pub., 1972.

[36] D. Bertsekas, *Dynamic Programming and Optimal Control*, 4th ed. Athena Scientific, 2012, vol. 2.

[37] M. Puterman, *Markov Decision Processes: Discrete Stochastic Dynamic Programming*, 1st ed. Wiley, 2005.

[38] S. Boyd and L. Vandenberghe, *Convex optimization*, 1st ed. Cambridge University Press, 2004.